NTNU

Norwegian University of
Science and Technology

Effect of Glutaminase Inhibition in Basal-Like Patient-Derived Xenografts Analyzed by Magnetic Resonance Spectroscopy

Ida Marie Henriksen

Master of Science in Physics and Mathematics
Submission date: June 2017
Supervisor: Bjørn Torger Stokke, IFY
Co-supervisor: Maria Tunset Grinde, ISB

Norwegian University of Science and Technology
Department of Physics

Preface

This Master's thesis was based on a collaboration between Department of Physics and Department of Circulation and Medical Imaging (MR Cancer Group) at the Norwegian University of Science and Technology, and was carried out during spring 2017.

I would especially like to thank my supervisor at MR Cancer Group, Postdoctoral Fellow Maria Tunset Grinde, for guidance and support with this thesis, and for the collaboration with the laboratory work, I am very grateful. I would also like to thank my supervisor at the Department of Physics, Professor Bjørn Torger Stokke, for guidance with the thesis, Postdoctoral Fellow Guro Fanneløb Giskeødegård for guidance with data processing and analyzes, and Senior Engineer Trygve Andreassen for help and guidance in the laboratory. Finally, I would like to thank MR Cancer Group for a very good professional and social environment the last year.

I alone have written this Master's thesis and performed analyzes, but all handling of living mice was performed by Postdoctoral Fellow Maria Tunset Grinde with valid laboratory animal science course.

Abstract

Breast cancer is today the leading cause for cancer related deaths among women in Europe. Decreased mortality among breast cancer patients has been observed over the last twenty years, where development and use of targeted therapies, utilizing hormone dependence, are believed to be part of the reason. Some subtypes of breast cancer still have poor prognoses for patients, where basal-like/triple-negative breast cancer (TNBC) patients have the worst predictions. Most basal-like tumors are triple negative, i.e. they lack expression of hormone receptors (estrogen (ER) and progesterone (PgR)) and human epidermal growth factor receptor 2 (HER2). Targeted treatment options for these patients are therefore limited, but use of glutaminase inhibitors have shown to be a potential treatment option for these patients. TNBC models have shown to be more dependent on L-glutamine and respond better to the glutaminase inhibitor CB-839 than ER-positive models, both in *in vitro* and *in vivo* xenograft models. CB-839 is currently under early stage clinical trials, but more information about the metabolic response of CB-839 in basal-like tumors is needed to identify patients likely to respond to treatment with CB-839. A patient-derived xenograft model named MAS98.12, displaying a basal-like/TNBC phenotype, has previously been established and is characterized in this study.

The aim of this study is to add more information about the metabolic response of CB-839 treated basal-like MAS98.12 tumors in mice. Tumor tissue and serum samples from CB-839 treated mice ($n = 6$) and control mice ($n = 5$) were harvested after injection of [5-^{13}C]L-glutamine. ^{13}C and ^{1}H MR spectra were acquired and analyzed by integration, multivariate analyzes (PCA and PLS-DA), and univariate analyzes (Student's t-test and Wilcoxon rank sum test). Significantly higher levels of L-glutamine were found in tumor samples treated with CB-839 than in controls, suggesting that CB-839 inhibits conversion from L-glutamine to L-glutamate. A previous study of CB-839 showed no effect on tumor growth in basal-like PDX model MAS98.12 when treated with CB-839. Overall, these results imply that MAS98.12 tumors are not dependent on L-glutamine for tumor growth. ^{13}C-labeled L-glutamate and L-lactate were also observed in the MR spectra of tumor tissue, but no significant differences were found between with CB-839 treated mice and controls. In serum samples, a significantly higher level of ^{13}C-labeled L-glutamine was also detected in CB-839 treated mice compared with controls, suggesting that CB-839 leads to a decrease in the overall uptake of L-glutamine from the bloodstream to other organs of the mouse.

Sammendrag

Brystkreft er den ledende årsaken til kreftrelatert død blant kvinner i Europa i dag. Synkende dødelighet blant brystkreftpasienter er observert de siste tjue årene, hvor utvikling av målrettet terapi som utnytter hormonavhengighet er antatt å være endel av grunnen. Noen undergrupper av brystkreft har fremdeles dårlige prognoser for pasientene, hvor pasienter med basal-lignende/trippel-negativ brystkreft har dårligst prognose. De fleste basal-lignende tumorer er trippel-negative, altså de mangler utrykk av hormonreseptorer (østrogen og progesteron) og human epidermal vekstfaktorreseptor 2. Målrettede terapimuligheter for disse pasientene er derfor begrenset, men bruk av glutaminasehemmere har vist å potensielt være en behandlingsmulighet for disse pasientene. Trippel-negative brystkreftmodeller har vist å være mer avhengig av L-glutamin og responderer bedre til glutaminasehemmer CB-839 enn ER-positive modeller, både i *in vitro* og *in vivo* xenotransplantasjonsmodeller. CB-839 er for øyeblikket i en tidlig fase av et klinisk studie, men mer informasjon om den metabolske responsen av CB-839 i basal-lignende tumorer er nødvendig for å identifisere pasienter som mest sannsynlig vil respondere til CB-839. En pasientavledet xenotransplantasjonsmodell kalt MAS98.12, som viser en basal-lignende/trippel-negative fenotype, har tidligere blitt etablert og er karakterisert i denne studien.

Målet med denne studien er å finne ut mer om metabolske responsen til basal-lignende MAS98.12 tumorer behandlet med CB-839 i mus. Prøver av tumorvev og serum fra CB-839-behandlede mus ($n = 6$) og kontrollmus ($n = 5$) var innhentet etter injisering av [5-^{13}C]L-glutamin. ^{13}C og ^{1}H MR-spektre ble tatt opp og analysert ved hjelp av integrering, multivariate analyser (PCA og PLS-DA) og univariate analyser (Students t-test and Wilcoxon rangsumtest). Et signifikant høyere nivå av L-glutamin ble funnet i tumorprøver behandlet med CB-839 sammenlignet med kontroller, noe som tyder på at CB-839 hemmer omdannelsen fra L-glutamin til L-glutamat. En tidligere studie av CB-839 viste ingen effekt på tumorvekst ved behandling med CB-839 i den basal-lignende pasientavledet xenotransplantasjonsmodell MAS98.12. Alt i alt tyder disse resultatene på at MAS98.12-tumorer ikke er avhengig av L-glutamin for tumorvekst. ^{13}C-merket L-glutamat og L-laktat var også observert i MR-spektrene av tumorvev, men det ble ikke funnet signifikant forskjell mellom CB-839-behandlede mus og kontroller. I serumprøver ble det også funnet et signifikant høyere nivå av ^{13}C-merket L-glutamin i CB-839-behandlede mus sammenlignet med kontroller, noe som tyder på at CB-839 fører til et minkende totalopptak av L-glutamin fra blodet til andre organer i musen.

List of abbreviations

α-KG	α-ketoglutarate
Ac-CoA	Acetyl coenzyme A
ATP	Adenosine triphosphate
CoA	Coenzyme A
ER	Estrogen receptor
$FADH_2$	Flavin adenine dinucleotide
FID	Free induction decay
FWHM	Full width half maximum
HER2	Human epidermal growth factor receptor 2
HMBC	Heteronuclear multiple bond correlation
HMDB	Human Metabolome Database
HR-MAS MRS	High-resolution-magic angle spinning MRS
LV	Latent variable
MR	Magnetic resonance
MRS	Magnetic resonance spectroscopy
NADH	Nicotinamide adenine dinucleotide
NOE	Nuclear Overhauser effect
NOESY	Nuclear Overhauser effect spectroscopy
OAA	Oxaloacetate
PC	Principal components
PCA	Principal component analysis
PDX	Patient-derived xenograft
PgR	Progesterone receptor
PLS	Partial least square
PLS-DA	Partial least square discriminant analysis
Q-Q plot	Quantile-quantile plot
rf	Radio frequency
SNR	Signal-to-noise ratio
SPSS	Statistical Package for the Social Sciences
TCA cycle	Tricarboxylic acid cycle
TN	Triple negative
TNBC	Triple negative breast cancer
TNM	Tumor, node, metastases

Contents

1 Introduction

Breast cancer is the most common type of cancer among women in Europe today [1]. Use of targeted endocrine therapy is one of the reasons why prognosis of breast cancer patients has become increasingly better over the last twenty years [2]. Still, patients with basal-like breast cancer have poor prognosis, partly because basal-like tumors are triple negative (TN) and then hormone independent, i.e. they lack expression of hormone receptors, estrogen (ER) and progesterone (PgR), and targeted endocrine therapy does therefore not work. Finding targeted therapies that utilize other properties than hormone dependence may therefore be beneficial to improve the prognosis of TNBC patients.

L-glutamine is essential for tumor growth in many cancer types [3]. L-glutamine is used to produce important metabolic intermediates in the tricarboxylic acid cycle (TCA cycle) and support production of adenosine triphosphate (ATP) [4]. Before L-glutamine can enter the TCA cycle, it must first be converted into L-glutamate and α-ketoglutarate. The conversion from L-glutamine to L-glutamate is catalyzed by the enzyme glutaminase, and elevated expression of glutaminase has been associated with high grade breast cancer [5].

Previous studies have shown that TNBC cell lines are especially dependent on L-glutamine compared to ER-positive cell lines [6] and more dependent on glycolysis compared to mitochondrial oxidative phosphorylation [7]. TNBC cells will therefore produce large amounts of L-lactate and L-alanine from glucose, resulting in only a small fraction of glucose entering the TCA cycle [3]. These cells may instead use L-glutamine as a source of energy and to produce metabolic intermediates in the TCA cycle [8].

A potential therapy for TNBC patients, which currently is in early stage clinical trials [9, 10], is use of the drug CB-839. CB-839 inhibits the enzyme glutaminase, which catalyze the conversion from L-glutamine to L-glutamate. The hope is that this drug will reduce access of important nutrients into the cancer cells and consequently stop cell proliferation and tumor growth. To this date, a preclinical study of CB-839 performed on basal-like/TN cell lines and animal models show that the basal-like/TN breast cancer subgroup is particularly dependent on L-glutamine, and that CB-839 inhibits proliferation and tumor growth in these models [6].

The basal-like patient-derived xenograft (PDX) model MAS98.12 has previously been established [11]. In another study, assessing glycolytic activity in MAS98.12 using ^{13}C magnetic resonance spectroscopy (MRS) and ^{13}C-labeled glucose, the glycolytic activity was found to be lower in the MAS98.12 tumors than in tumors from a luminal-like/ER-positive PDX model MAS98.06 [12]. Tumor growth of MAS98.12 treated with CB-839 has also been measured in another study (unpublished results) and the result show no significant decrease in tumor growth in CB-839 treated compared with controls (see appendices Figure E.1).

The aim in this study is to add more information about the metabolic response to CB-839 in the basal-like PDX model MAS98.12 to better understand the mechanisms behind CB-839 and the impact it has on metabolism in tumor tissue. The end products of L-glutamine will be traced by injecting [5-^{13}C]L-glutamine in CB-839 treated and untreated mice with basal-like MAS98.12 tumors. Serums and tissue samples will be analyzed using ^{1}H and ^{13}C MRS.

2 Theory

2.1 Cancer

Formation of cancer, oncogenesis, is a process where normal cells are transformed into cancer cells after multiple mutations in DNA, leading to dynamic changes of the genome that makes the cells proliferate and grow uncontrolled [13]. Cancer cells can behave very differently, but there are some common hallmarks that are essential for transforming any normal cell into a cancer cell. These hallmarks include self-sufficiency in growth signals, insensitivity to anti-growth signals, tissue invasion and metastasis, limitless replicative potential, sustained angiogenesis, and evading apoptosis [13, 14]. In addition, there is also a discussion if reprogramming of energy metabolism should be included as a hallmark, because cancer cells have found to have a different glycolytic and glutamine metabolism of cell membrane than normal cells growing with the same growth rate [15].

2.2 Breast cancer

Breast cancer is the second most diagnosed type of cancer worldwide today [16], and the leading cause of cancer related deaths among European women [1]. 25.2 % of all cancer diagnosis of women in 2012 were of breast cancer, where in total 1.67 million women were diagnosed [16]. Still, the mortality of breast cancer has decreased in European countries over the last twenty years [2], where the reason is believed to be a combination of use of mammography, for women in the age of 50-69 years old [1], and use of targeted hormone treatment [17]. Hormone treatment can only be used on hormone dependent breast cancer, so hormone independent breast cancer still has limited treatment options.

2.2.1 Subtypes of breast cancer

Breast cancer is a heterogeneous disease, and is a common term for many different diseases in the breast with variations of molecular aberrations [18]. There are different ways of characterizing the varying types of breast cancer. In clinic, breast cancer is often divided into subtypes based on the presence or absence of molecular markers and is classified as ER-positive/negative, PgR-positive/negative, in the amount of the human epidermal growth factor receptor 2 (HER2), and the Ki-67 score [19]. Another classification is based on the genetic expression patterns between cases of breast cancer. This classification look for similarities in gene expression that reflects the molecular differences in breast cancer cells. These subtypes are called molecular subtypes and are divided into luminal A, luminal B, basal-like, HER2-type, and normal-like breast cancer, where each group can be looked at as separable diseases with different treatments options, prognosis, and overall survival, see Figure 2.1 [19, 20].

Luminal breast cancer is the most common type of breast cancer, with the best prognosis for the patients [20, 21]. Luminal tumors are often ER-positive and/or PgR-positive,

which means that they are dependent on hormones to grow. Luminal A tumors are often also HER2-negative with low Ki-67 score, while luminal B tumors can be either HER2-positive or HER2-negative with high Ki-67 score [22]. Since these tumors are dependent of hormones, they can be inhibited by hormone blockers, which can be used for targeted endocrine therapy. Use of endocrine therapy is one of the reasons why luminal breast cancer patients have relatively good prognosis [23], as shown in Figure 2.1.

Basal-like breast cancer is an aggressive type of breast cancer that overlap TNBC, with a discordance of 20-30 % [19, 24]. TNBC is ER-negative, PgR-negative, and HER2-negative and is therefore independent of hormones to grow. Because basal-like breast cancer often is triple-negative they are also independent of hormones, which means that they cannot be inhibited by hormone blockers and cannot be treated with targeted endocrine therapy. The prognosis when having basal-like breast cancer is today very poor, as shown in Figure 2.1, because the cancer is aggressive and it does not exist any targeted treatment for this subtype of breast cancer [21, 25].

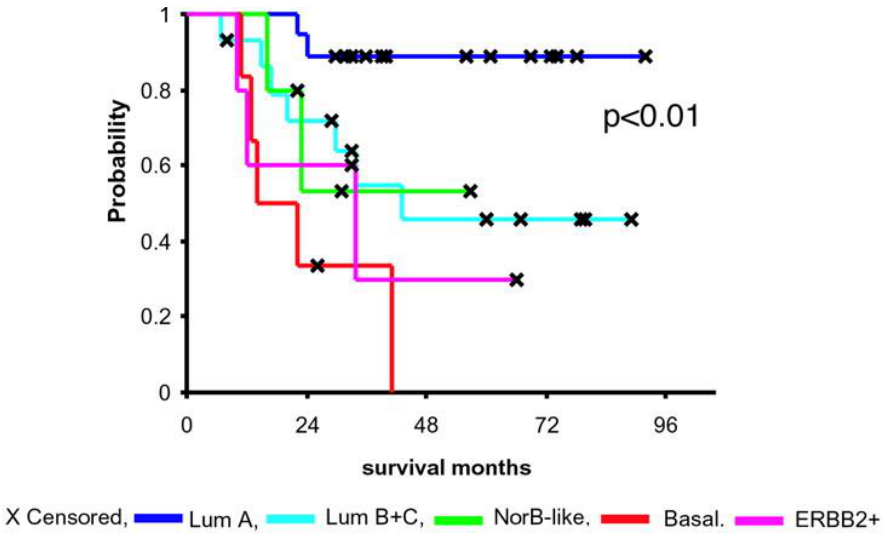

Figure 2.1: Overall survival of patients with luminal A, luminal B, basal-like, normal-like, and HER2 type breast cancer. Adapted from Sørlie [20], and printed with permission from the National Academy of Sciences, U.S.A (Copyright 2001).

2.2.2 Diagnosis and prognosis of breast cancer

Diagnosis of breast cancer is normally performed by staging the cancer, which describes the extent of cancer and the prognosis of the patient. The most commonly used system is the tumor, node, metastases (TNM) staging system, which stages the cancer based on the primary tumor size, the regional lymph node involvement, and the presence of distant

metastasis [26]. From this system, breast cancer is staged from 0 to IV, where stage 0 is non-invasive breast cancer, stage I-III are invasive breast cancer, and stage IV is breast cancer with dissemination to other organs [1].

Prognostic factors of breast cancer are factors that can predict the clinical outcome at the time of diagnosis. Staging breast cancer through the TNM staging system is a prognostic factor, where the lymph node status is the most significant prognostic indicator [27]. The presence of the molecular markers ER, PgR, and HER2 are also important prognostic factors, because they are the main indicator for the response to endocrine therapy, where the presence of ER and PgR indicates good response to endocrine therapy [28].

2.3 Patient-derived xenograft models

Animal models are often used to study human breast cancer. Most *in vivo* models are based on cell lines that are isolated from human breast tumors and selected in culture before being implanted into immunodeficient mice [11]. These models have shown to possibly loose some of the heterogeneity of the original tumor [11]. PDX models are animal models where primary tumor tissue, originating from humans, is directly implanted into immunodeficient animals, in particularly mice [29, 30]. The advantage of using PDX models is that the implanted tumors maintain similarities to primary human tumors like the histopathology, clinical markers, and gene expression profiles [29, 31]. PDX tumors can be engrafted heterotopically or orthotopically [32]. Heterotopic models are the easy choice, where a tumor is implanted into the subcutaneous flank of mice. This gives easy cell transfer and monitoring of cell growth and location [33]. Orthotopic models are more technically challenging and more time consuming, where the tumor is implanted directly into an organ of choice [33]. The benefit of using an orthotopic model is that it is more accurate to human tumors, most likely due to more similar microenvironment, and is found to have more similarities in histology and gene expression profiles to human tumors than heterotopic models [34].

2.4 Cancer metabolism

Cells need energy in form of ATP to maintain cell growth and proliferation. Under aerobic conditions of normal cells, the production of ATP is supported by glucose. Glucose produces pyruvate through the glycolysis and can enter the TCA cycle, which produces nicotinamide adenine dinucleotide (NADH) and flavin adenine dinucleotide ($FADH_2$) that can be used to produce ATP through the oxidative phosphorylation [35]. To adjust for increased proliferation, cancer cells have changed their energy metabolism. Pyruvate produced from glucose is then to a high degree used to produce lactate and alanine, under aerobic conditions, instead of entering the TCA cycle. This change in metabolism is called the Warburg effect and is a less efficient way of producing ATP [4, 13]. A possible explanation for this change in metabolism is the increased production of lactate that can be released into the extracellular domain, making the tumor more invasive by disrupting the

architecture of normal tissue [36]. Cancer cells have in addition altered uptake of amino acids compared with normal cells, especially increased uptake of glutamine have been found for rapidly proliferating cells [3].

2.4.1 Glutamine dependence in cancer cells

Glutamine is a conditional amino acid, which means that supply of glutamine is only essential under special conditions. Normal cells can provide itself with the necessary amount of glutamine from glucose and are therefore not dependent of any supply of glutamine from sources outside the cell. For some cancer cells glucose is not sufficiently supporting the TCA cycle [37, 38]. Glutamine has then shown to be an essential amino acid because it can support the TCA cycle through the glutaminolysis [3].

Glutaminolysis is the metabolic breakdown of glutamine. A part of the glutaminolysis leads to metabolites that enter the TCA cycle, where ATP and biosynthetic intermediates can be catabolized. Parts of the glutaminolysis are illustrated in Figure 2.2. Glutaminolysis starts with glutamine being deaminated, by the mitochondrial enzyme glutaminase, making glutamine donate a nitrogen to ammonia and convert into glutamate [39]. Glutamate can then go into different pathways, where in one pathway glutamate is oxidized into α-ketoglutarate (α-KG), a product in the TCA cycle, in a process that simultaneously converts pyruvate into alanine. Pyruvate can also produce malate and be converted into lactate [40]. α-KG can enter the TCA cycle, which produces NADH and $FADH_2$ that through the oxidative phosphorylation can produce ATP [3, 41]. Another pathway for glutamate is through the glutamate/cystine antiporter, x_c^-, that pumps one glutamate out of the cell and into the extracellular domain, while pumping one cystine into the cell [8, 42]. When inside the cell, cystine is converted into cysteine that can be used to synthesize the antioxidant glutathione together with glutamate and glycine [43]. Production of glutathione is important for cancer cells to withstand oxidative and free radical damage [44].

Cancer cells have also shown to have larger glutamine pools than normal cells, and because these cells often cannot supply themselves with necessary amount of glutamine, it must come from other sources like de novo synthesis, the blood supply, or reduced transport to normal astrocytes [45]. Examples of important macromolecules produced through the glutaminolysis are cholesterol and fatty acids, which are dependent on citrate and amino acids, and lipids and nucleotides, where ATP is essential for synthesis [3, 4, 46, 47].

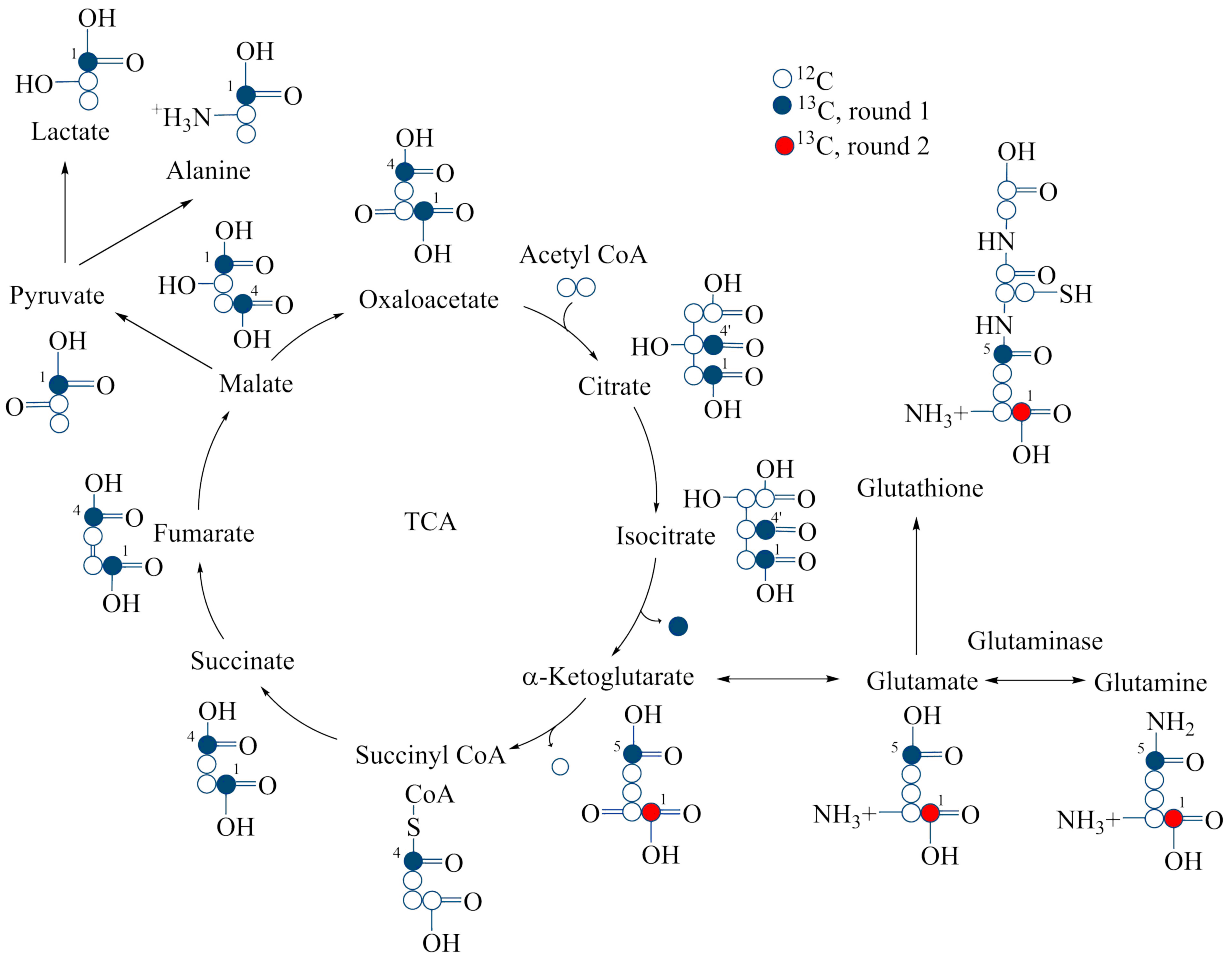

Figure 2.2: Illustration of [5-^{13}C]glutamine metabolism in the TCA cycle. L-glutamine labeled with ^{13}C in fifth position will stay in fifth position when converted into glutamate, with help of the enzyme glutaminase [39]. Glutamate can be used to produce glutathione [43] or α-ketoglutarate (α-KG), a product in the TCA cycle. In the TCA cycle, ^{13}C-labeled carbon can be in two different positions when going from succinyl coenzyme A (succinyl CoA) to succinate. When converted into malate, some of the malate goes further into the TCA cycle, producing oxaloacetate, and some can be used to produce pyruvate and then lactate and alanine [40], with the ^{13}C-labeled carbon in first position. Further in the TCA cycle, acetyl coenzyme A (Ac-CoA) is added forming citrate. When going from citrate back to α-KG, ^{13}C-labeled carbon leaves the TCA cycle in one of the configurations. In the other configuration, the ^{13}C-labeled carbon will be in first position of α-KG and stay in first position when converted back to glutamate and glutamine [4].

2.5 ^{13}C-labeling of glutamine

Most carbon atoms are ^{12}C and only 1.1 % are ^{13}C. It is therefore possible to ^{13}C-label molecules containing carbon atoms by replacing a specific ^{12}C isotopes with ^{13}C isotopes.

^{13}C-labeled molecules, and its downstream metabolites, can then be detected using ^{13}C MRS [12]. Glutamine contains five carbon atoms and it is possible to ^{13}C-label one or more carbon atoms on glutamine.

^{13}C-labeling carbon number five on glutamine, see Figure 2.2, will make the ^{13}C-labeled carbon stay in the fifth position when converted from glutamine to glutamate and then into α-KG. In the conversion from α-KG to oxaloacetate (OAA), the carbon in first position leaves the cycle, resulting in a four carbon OAA that can have two different configurations [4]. The ^{13}C-labeled carbon can then be in either first or fourth position of OAA. In the conversion from OAA to citrate, acetyl coenzyme A (Ac-CoA) is added, making a five-carbon chain with a branched carbon. When going from citrate to α-KG the carbon on the branch will leave the cycle, so for one of the configurations the ^{13}C-labeled carbon will leave the TCA cycle. For the other configuration, the ^{13}C-labeled carbon will be in first position of α-KG and will stay in first position when converted to glutamate and then glutamine [4]. It is therefore possible to detect metabolites from the whole TCA cycle by using ^{13}C MRS when ^{13}C-labeling carbon number five on glutamine.

2.6 Glutaminase inhibition for treatment of TNBC

TNBC cells are associated with elevated glutaminase activity [48]. Since glutaminase catalyzes the conversion from glutamine to glutamate, this suggests that TNBC cells are dependent on glutamine metabolism to get essential intermediates from the TCA cycle that are important for cell growth [48]. Inhibiting glutaminase is therefore believed to decrease and possibly stop cell growth of TNBC cells [3, 48].

On type of glutaminase inhibitor is Calithera's glutaminase inhibitor CB-839, illustrated in Figure 2.3. The enzyme glutaminase is a tetramer with four binding sites and CB-839 binds to the glutamine binding pocket on glutaminase and changes the loops of glutaminase to prevent glutamine from binding [6, 47]. The characteristics of CB-839 are that it is orally bioavailable, potent, selective, and has a time-dependent reversible inhibition with a slow recovery time [47].

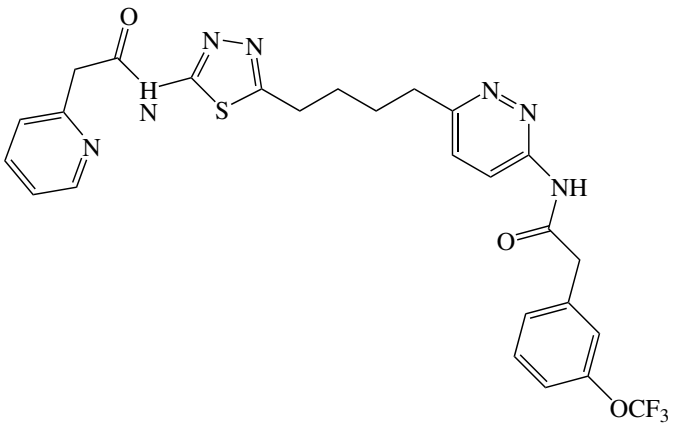

Figure 2.3: Structure of glutaminase inhibitor CB-839 as described in [49] at reference #670.

2.7 Magnetic resonance spectroscopy

MRS utilizes the magnetic moment of nuclei with spin $I = \frac{1}{2}$, such as ^{1}H and ^{13}C. These nuclei may exist in two different energy states at slightly different energy levels. In the presence of an external magnetic field, a small majority of these nuclei will align in the direction of the external magnetic field with the lowest energy state. A majority of total spins in the direction of the magnetic field, will lead to a small magnetization vector in this direction that can be further utilized [50].

When a radio frequency (rf) pulse is applied, it will be absorbed by nuclei with a rotational frequency corresponding to the frequency of the applied rf pulse [51]. The rotational frequency, ν, of a nuclear spin is dependent of the experienced magnetic field strength, B_0, and is given by

$$\nu = \gamma \cdot B_0, \tag{1}$$

where γ is the gyromagnetic ratio of the given nucleus. The experienced external magnetic field of a nucleus is dependent on the degree of shielding from the external magnetic field it experiences from nearby electrons, which is determined by the chemical environment of the given nucleus. Two identical nuclei with different chemical environment will therefore, from Equation (1), have different rotational frequencies and will therefore absorb energy at different frequencies. When an rf pulse is applied, spins with corresponding frequencies will be knocked out of alignment with the external magnetic field and will relax back to thermal equilibrium by spin-lattice interactions, leading to longitudinal relaxation (T_1), and spin-spin interactions, leading to transverse relaxation (T_2) [52]. This relaxation can be detected by a coil as a signal decay, called the free induction decay (FID). The FID signal can then be Fourier transformed to reveal the frequency signal [51], and the amount of different frequencies can be detected. The results can be represented in a magnetic resonance (MR) spectrum that can be analyzed to investigate which metabolites are present in a sample

and the amount of each metabolite [51].

2.7.1 Chemical shift scale

MR spectra are represented with a chemical shift scale. Chemical shift, δ, is defined as the difference between the resonance frequency of a nucleus of interest, ν_{sample}, and the resonance frequency of a reference nucleus, ν_{ref}, and can be expressed by

$$\delta(\text{ppm}) = 10^6 \cdot \frac{\nu_{\text{ref}} - \nu_{\text{sample}}}{\nu_{\text{ref}}}$$

Chemical shift is a measure without unit that is independent of the magnetic field strength in the system [51].

2.7.2 Spin-spin coupling

Spin-spin coupling occurs when the magnetic moment of neighboring nuclei affect each other. This effect is mediated by the bonding electrons and is determined by the distance between the nuclei, the type of chemical bond, the bond angle, and the nuclear spin [51]. Spin-spin couplings are shown as splitting of peaks into multiplets in MR spectra, where the number of peaks in a multiplet gives information about the number of close neighboring nuclei to the detected nucleus [51].

2.7.3 Chemical exchange

A molecule may exist as different conformational isomers, called conformers, where rotation around single bonds creates different isomers of a molecule. A given molecule will have a dynamic equilibrium of conformers, where the molecule may switch between different conformations [53]. A nucleus in a molecule will have different chemical environment for different conformations and will therefore be detected at different chemical shifts. If the conformation change is slow compared with the acquisition time, the signal from the different conformations will be observed as separable peaks in MR spectra. This effect is called slow-chemical exchange and occurs often at lower temperatures [54]. If conformation change is fast compared with an acquisition, the molecule will be in both conformation within the acquisition and the signal from all conformation will be detected as a singlet at the same chemical shift in MR spectra. The chemical shift of the molecule will correspond to the average of the chemical shifts of the detected conformations. This effect is called fast-chemical exchange and occurs often at higher temperatures [54]. ^{13}C MRS is more sensitive to conformation changes than ^{1}H MRS, because larger chemical shift differences in ^{13}C MR spectra makes it easier to detect conformation changes [55].

2.7.4 Shimming

It is desired that the magnetic field is as homogeneous as possible, because it leads to higher spectral resolution in MR spectra. When a sample is placed into a magnet, the

content in the samples will make small inhomogeneities to the magnetic field that will decrease the resolution in resulting MR spectra. In attempt to make the magnetic field more homogeneous, shimming is performed after a sample is placed into the magnet by adjusting the current in shimming coils. Successful shimming leads to higher and more narrow peaks in MR spectra [56]. Full Width Half Maximum (FWHM) is often used on a singlet in the MR spectrum to decide when the shimming is good together with looking at the symmetry of peaks. Depending on the sample content, a limit for desired FWHM is decided.

2.7.5 High-resolution-magic angle spinning MRS

High-resolution-magic angle spinning MRS (HR-MAS MRS) has shown to be a good technique for monitoring metabolism in biological tissue [57, 58]. HR-MAS MRS spins a sample around a given angle to the external magnetic field, called the magic angle θ_{MA} [59], to cancel effects from interactions such as chemical shift anisotropy and dipole-dipole coupling. In liquids, molecular motions cancel out these effects, while in tissue, molecules are more bound, so these effects are not canceled, which makes peaks in MR spectra broader. To limit these effects in tissue, the probe with the sample can be rotated with an angle θ_{MA} that averages to zero the broadening effects. These effects have shown to have an angular dependence described by $3\cos^2\theta - 1$, and will be canceled if equal zero. θ_{MA} is then found by solving $3\cos^2\theta_{\mathrm{MA}} - 1 = 0$ with respect to θ_{MA}, and θ_{MA} is found to be 54.7° [57, 60]. By rotating a rotor with a tissue sample around the sample spinning axis at an angle of 54.7°, compared with the static magnetic field B_0 as illustrated in Figure 2.4, the MR spectral line-widths will decrease and will lead to higher resonance, and then a higher spectral resolution, in the resulting MR spectra [59, 60, 61].

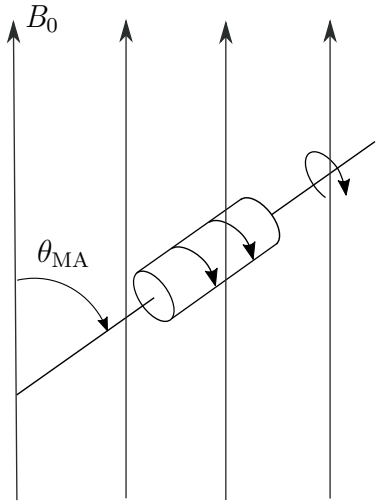

Figure 2.4: Illustration of a sample rotating with a degree of θ_{MA} compared to the external magnetic field B_0.

2.7.6 ^{13}C HR-MAS MRS

When using MRS, it is possible to target and detect signal from different nuclei with spin $\frac{1}{2}$. Because different nuclei, like ^{1}H and ^{13}C, have different gyromagnetic ratio, they will from Equation (1), also have different rotational frequencies. Different coils must therefore be used to detect signal from different nuclei in an MR system. MRS usually targets ^{1}H nuclei because ^{1}H nuclei have a high natural abundance in the human body and because ^{1}H nuclei have a high gyromagnetic ratio (γ) compared to other nuclei, making it a more sensitive nucleus in MRS. ^{13}C nuclei have a lower gyromagnetic ratio than ^{1}H and give therefore lower sensitivity in MRS ($\gamma_{13\mathrm{C}} \approx \frac{1}{4}\gamma_{1\mathrm{H}}$). There is also a low natural abundance of ^{13}C with 1.1 % of all carbon isotopes. In despite of the low sensitivity when using ^{13}C MRS, it is beneficial to use this method in some cases, because of the possibility to investigate metabolic pathways by following ^{13}C-labeled substrates in cell cultures or animals. In ^{13}C MR spectra the spectral resolution is also much higher ($\sim$ 220 ppm) than for ^{1}H MR spectra ($\sim$ 15 ppm) and peaks are therefore easier to separate [62]. ^{13}C MRS has therefore shown to be a good tool for studying ^{13}C-labeled substrates with downstream metabolites in glycolysis, TCA cycle, or other metabolic pathways [12]. All carbon atoms on glutamine can be ^{13}C-labeled, and different labeling will lead signal at different frequencies in resulting MR spectra. An example of a ^{13}C HR-MAS MR spectrum from mice injected with ^{13}C-labeled [5-^{13}C]glutamine is shown in Figure 2.5 with identified metabolites.

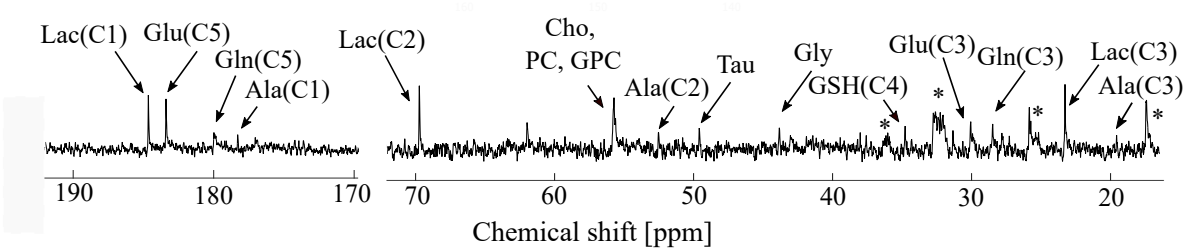

Figure 2.5: Example ^{13}C HR-MAS MR spectrum of basal-like PDX tissue injected with ^{13}C-labeled glutamine and with identified metabolites, where (*) represents fatty acids. Ala: alanine, Cho: choline, gln: glutamine, glu: glutamate, GPC: glycerophosphocholine, GSH: glutathione, gly: glycine, lac: lactate, PC: phosphocholine, tau: taurine.

2.7.7 Pulse sequences

The main purpose of a pulse sequence is to give out the best signal possible in MR spectra, with optimal signal-to-noise ratio (SNR) and suppression of unwanted signals. The optimal pulse sequence is dependent on the experiment.

1D nuclear Overhauser effect spectroscopy (1D NOESY) pulse sequence utilizes the nuclear Overhauser effect (NOE). NOE is the cross-relaxation between two spins by transfer of spin polarization. This effect can be used to saturate one peak while measuring the effect of another, so one ^{1}H peak can be measured at the time. A reason for using 1D NOESY pulse sequence is that it easily suppresses the water signal and little optimization is needed [63]. In addition, 1D NOESY pulse sequence is quantitative and is therefore good for comparing peaks within an MR spectrum [64].

^{13}C single pulse with ^{1}H decoupling pulse sequence can be used for detection of only the signal from ^{13}C. It is a 1D pulse sequence, where the ^{1}H is decoupled by continuously exciting ^{1}H with repeating pulses, making the multiplets collapse into a singlet and increasing the SNR in MR spectra [64]. The drawback with this pulse sequence is that it is not quantitative, but this gives a much shorter repetition time. For 1D quantitative ^{13}C MR spectra, a pulse sequence with inverse gated decoupling can be used [64].

2.8 Preprocessing and analysis of MRS metabolomics data

2.8.1 Preprocessing MRS metabolomics data

Before statistical analyzes can be implemented, MRS metabolomics data is preprocessed to avoid instrumental and experimental artifacts [65]. Raw MR spectra may include differences due to other factors than biological characteristics, like change in signal intensities in MR spectra due to variations in sample mass or higher or lower chemical shifts in MR

spectra due to temperature and pH changes. These artifacts can be reduced by preprocessing MRS metabolomics data by computational procedures before analyzed. Normal procedures of preprocessing MRS metabolomics data are baseline correction, normalization, peak alignment, and mean centering [65].

One way of performing baseline correction is using the method asymmetric least square that uses the least square algorithm to fit a baseline. This is carried out by making a vector of weights and minimize the residuals, and adding a term to smooth the estimated baseline [65]. The standard for normalization of MR spectra of tissue samples, is area normalization that gives all MR spectra the same area by dividing each data point by the equal total area [65]. For serum samples, area normalization is usually not performed on MR spectra before univariable analysis [66], instead samples can be corrected for varying variables, like sample mass. Peak alignment of MR spectra can be performed by using icoshift, where intervals around all peaks are selected and each interval is co-shifted by using fast Fourier transform to give the best correlation between MR spectra [67]. Mean centering is performed to get values in MR spectra to vary around zero, instead of the mean metabolite value [68]. This is carried out by subtracting the column mean intensity from each individual intensity value. The origin of each component, found by using principal component analysis (PCA), will then be in the centroid of the data [69].

2.8.2 Multivariate analysis

Multivariate analysis is a statistical method for analyzing data with more than one variable at the time. Multivariate analysis takes advantages of the correlation between variables to reduce the number of variables into fewer uncorrelated variables. Multivariate analysis can be divided into two categories, supervised and unsupervised. Supervised classification uses prior knowledge about the data to find predictions or classifications, while unsupervised classification does not use prior knowledge about the data and try to discover new patterns [70].

Principal component analysis
PCA is an unsupervised multivariate analysis that uses orthogonal transformation to find linearly uncorrelated variables, called principal components (PC), from possibly correlated variables. All PCs are orthogonal to each other and are organized so the first PC has the highest variance and the next PCs have the highest variance it can have while still being orthogonal to the preceding PCs. The result is a vector consisting of an uncorrelated orthogonal basis set, which is a linear combination of the original variables. Each PC also has a corresponding loading profile that describes the importance of the original variable for the new PC [71].

Partial least square
Partial least square (PLS) is a supervised clustering multivariate analysis [72, 73]. PLS look for fundamental relations between two matrices expressed by latent variables (LVs)

that maximizes the covariance between the matrices. PLS discriminant analysis (PLS-DA) is a special case of PLS that attempts to find a discriminant between two classes using "dummy" variables to represent each class [74]. Permutation test is a method of cross-validation used to validated if the classification found by PLS-DA is significantly different from random to avoid overfitting or underfitting the classification. A permutation test is performed by randomly label all samples and performing the same test as for the original data sets [74]. This is repeated n times, where the p-value of the test is found by

$$p = \frac{\text{error}}{n} \tag{2}$$

where error is the number of classification errors found by the permutation test [75].

2.8.3 Univariate analysis

Univariate analysis is a statistical analysis used for analyzing data with only one variable. Dependent on the properties of the data sets different analyzes are preferred.

Student's *t*-test
Student's t-test is a univariate analysis that determines if the difference, in mean values between two groups with non-dependent data, is significant or non-significant [76]. This test requires that all outliers in the data are removed and that the data sets are reasonable normally distributed. For an extremely small sample size, $n \leq 5$, Student's t-test can be used if the effect size is expected to be large [77]. A t-value, for a data set with n samples, can calculated from the formula [78],

$$t = \frac{\mu_1 - \mu_2}{s_p^2 \sqrt{\frac{1}{n_1} + \frac{1}{n_2}}},$$

where μ_i is the mean value of the normal distributed data set i and s_p^2 is the pooled variance and is calculated from the formula

$$s_p^2 = \frac{(n_1 - 1)s_1^2 + (n_2 - 1)s_2^2}{n_1 + n_2 - 2},$$

where s_i is the standard deviation of data set i equal to

$$s_i = \sqrt{\frac{\sum_{j=1}^{n_i}(x_j - \bar{x})^2}{n_i - 1}}.$$

The p-value of Student's t-test can be found by taking the area of the tail from the t-value, on one or both sides of the normal distribution of the data set, dependent on the test being one-tailed or two-tailed. If the calculated p-value, between two data sets, is less or equal to the significance level, α, normally chosen to be 0.05, the difference between the two data sets classifies as significant [76].

Wilcoxon rank sum test
If a data set is not normally distributed and the samples in the data set are not dependent, a Wilcoxon rank sum test is often preferred [79]. This analysis combine two data sets and range the data based on magnitude, where each sample get a range from 1 to the sum of the two data sets. The sum of all ranks in a data set is then calculated for each data set and compared and the p-value of the test can be found by using the table in Wilcoxon [79]. As for the t-test, if the p-value is less or equal to the significance level the difference between the two data sets is classified as significant [76, 79].

Determination of normal distribution
Normal distribution of a data set can be visually decided by illustrating the data in a normal quantile-quantile (Q-Q) plot. A Q-Q plot compares two distributions, and if they are similar they will make a straight line at $y = x$. A normal Q-Q plot will compare the observed value of the data points against the expected normal value to determine if the data points are normally distributed [80].

Dixon-type test
Before univariate analysis can be performed outliers must be removed. To decide if extreme values found in a data set is classified as outliers, a Dixon-type test is preferred for small samples sizes, $n < 10$. Dixon-type test look at the ratios between the range in a data set, with n samples, to decide if a possible outlier is outside the expected range. The ratio, when the outlier, x_n, is the highest value in the data set, is decided from the formula

$$r_{10} = \frac{x_n - x_{n-1}}{x_n - x_1} \tag{3}$$

where the data set in ranged from lowest to highest value and x_1 is the lowest value in the data set. If the calculated r_{10} is higher than a critical value found in Dixon [81], which is dependent on the number of samples n and the significance level, the value is classified as an outlier.

3 Materials and methods

This study includes acquisition and analyzes of MRS metabolomics data of serum and tissue from the basal-like PDX model MAS98.12 of immunodeficient mice injected with [5-^{13}C]L-glutamine both treated with CB-839 ($n = 6$) and controls ($n = 5$), and immunodeficient mice with only natural abundance ($n = 3$). Table 3.1 shows an overview of materials, methods, and analyzes used in this study. All procedures and experiments involving animals were approved by the National Animal Research Authority (FOTS ID: 9126).

Table 3.1: Overview of materials, methods, and analyzes used in this study of basal-like PDXs of immunodeficient mice injected with [5-^{13}C]L-glutamine both treated with CB-839 ($n = 6$) and controls ($n = 5$), and of mice with only natural abundance ($n = 3$).

	Materials	Methods	Analyzes
CB-839 treated ($n = 6$)	Tissue	^{1}H HR-MAS MRS	PCA
			PLS-DA
		^{13}C HR-MAS MRS	Mean spectrum
			Integration
			PCA
			Student's t-test
			Wilcoxon rank sum test
	Serum	^{13}C MRS	Integration
			PCA
			Student's t-test
			Wilcoxon rank sum test
Controls ($n = 5$)	Tissue	^{1}H HR-MAS MRS	PCA
			PLS-DA
		^{13}C HR-MAS MRS	Mean spectrum
			Integration
			PCA
			Student's t-test
			Wilcoxon rank sum test
	Serum	^{13}C MRS	Integration
			PCA
			Student's t-test
			Wilcoxon rank sum test
Natural abundance ($n = 3$)	Tissue	^{13}C HR-MAS MRS	Mean spectrum

n: number of samples, HR-MAS MRS: high-resolution-magic angle spinning magnetic resonance spectroscopy, PCA: principal component analysis, PLS-DA: partial least square discriminant analysis.

3.1 Animal and sample handling

In this study, tissue and serum samples from mice representing the basal-like PDX model, MAS98.12, were obtained and analyzed. MAS98.12 tumors were already orthotopically implanted in the mammary fat pad by others, as described in Bergamaschi [11]. These tumors have shown to maintain the characteristics of a basal-like breast tumors, TN breast tumors, and to have a similar gene expression as the basal-like phenotype [11]. All mice used in experiments were female, at equal age, and with similar mass of 27.9 g ± 2.0 g at the time of experimentation (all mice masses are represented in appendices Table A.1).

3.1.1 Administration of CB-839

CB-839 (developed by Calithera BioSciences, USA) dissolved in a drug vehicle (20 mg/ml in 10 % cyclodextrin in saline) was administrated (200 mg/kg) twice a day, morning and afternoon, for two days. Doses were administered perorally per gavage with a total volume of 0.25 ml. Control mice received a volume-matched drug vehicle (10 % cyclodextrin in saline) using the same procedure as for CB-839 treated mice.

3.1.2 [5-^{13}C]L-glutamine injection

Serum and tissue samples were obtained by first weighing the mice and put them into an incubation chamber filled with isoflurane (2 %), N_2O, and O_2, until they were sleeping. After the mice were fast asleep, they were put on a mask with the same gas content. L-glutamine solution, containing 35 mg/ml L-glutamine, labeled with ^{13}C on carbon number five (99 % [5-^{13}C]L-glutamine, Cambridge Isotope, Andover USA), was injected into the tail veins of the mice using an injection pump (AlarisCC) that controls the rate of L-glutamine infused into the mice. Doses given to the mice were adjusted for the body mass of the mouse m_{mice}. The first three minutes a total dose, $d_{3\text{min}}$, of

$$d_{3\text{min}}(\text{mg}) = m_{\text{mice}}(\text{g}) \cdot 0.3 \text{ mg/g}$$

was administrated. The next three hours a total dose, $d_{3\text{h}}$, of

$$d_{3\text{h}}(\text{mg}) = m_{\text{mice}}(\text{g}) \cdot 0.005 \text{ mg/(g} \cdot \text{min)} \cdot 180 \text{ min}$$

was continuously administrated.

3.1.3 Sample collection

After injection, the mice were sacrificed by cervical dislocation and the tumors were immediately collected and stored in liquid nitrogen (77 K) until sample preparation. Blood was collected from the right ventricle of the mice using a 25-27 G needle and stored in room temperature for 20 minutes until blood clots were formed. The blood was then centrifuged for 10 minutes, and serum was collected and stored in liquid nitrogen (77 K) until sample preparation.

3.2 Magnetic resonance spectroscopy

Overview of MRS protocol used on tissue and serum samples of basal-like PDXs are shown in Table 3.2.

Table 3.2: Method, spectrometer, pulse program, and MR acquisition parameters used for acquisition of MR spectra of tissue and serum samples of basal-like PDXs.

	Tissue samples		Serum samples
Method	^{13}C HR-MAS MRS	^{1}H HR-MAS MRS	^{13}C MRS
Spectrometer	Bruker Avance III 600 MHz	Bruker Avance III 600 MHz	Bruker Avance III 600 MHz Ultrashield Plus
Pulse program	Single pulse with ^{1}H decoupling zgpg30; Bruker	1D NOESY noesygppr1d; Bruker	Single pulse with ^{1}H decoupling zgpg30 ; Bruker
Parameters:			
Spin rate	5 kHz	5 kHz	5 kHz
Flip angle	30°	90°	30°
NS	16384	128	2048
AQ	0.87 sec	2.74 sec	1.65 sec
T_R	1.87 sec	6.74 sec	2.15 sec
Sweep width	29.9 ppm/18 kHz	251 ppm/38 kHz	197 ppm/30 kHz
Temperature	277 K	277 K	301.5 K
Total time	8 h 45 min	15 min	1 h 15 min

HR-MAS MRS: high-resolution-magic angle spinning magnetic resonance spectroscopy, NOESY: nuclear Overhauser effect spectroscopy, NS: number of scans, AQ: acquisition time, T_R: repetition time.

3.2.1 Preparation and acquisition of tissue samples

Tissue samples (37.2 mg ± 2.6 mg) from basal-like PDX model MAS98.12 were cut into a proper size to fit a 50 μl rotor on a block cooled in liquid nitrogen to minimize degradation of the sample under preparation. 16 μl of a lock reference, containing 99.9 % D_2O (CDN isotopes, Pointe-Claire, Canada) and 25 mM sodium formate (Sigma-Aldrich, Shanghai, China), was added in the rotor together with the tissue sample. The rotor was then closed with a plug and fasten with a screw and inserted into a magnet, where the rotor was aligned at the magic angle of 54.7 ° to the magnetic field. All samples were shimmed using formate in the ^{1}H MR spectrum, until the FWHM was less than 1.5 Hz (all FWHM are represented in appendices Table A.1). MR spectra were acquired using a Bruker Avance III 600 MHz (Bruker BiosSpin GmbH, Rheinstetten, Germany) equipped with a 4 mm ^{1}H/^{13}C HR MAS probe, with acquisition parameters listed in Table 3.2. MR spectra were

processed using a line broadening of 1.0 Hz for ^{13}C MR spectra and 0.3 Hz for ^{1}H MR spectra.

3.2.2 Preparation and acquisition of serum samples

Serum samples were thawed and 50 μl of the serum was mixed with 200 μl of a serum lock reference containing 0.075M $Na_2HPO_4\times$ $7H_2O$, 4 % NaN_3, and 0.08 % TSP (3-(trimethylsilyl)propionic acid-d4, Aldrich), mixed in H_2O (80 %) and D_2O (20 %, CDN isotopes, Pointe-Claire, Canada). Serum samples were then transferred into a high-quality 3 mm NMR tube. ^{13}C MR spectra were acquired using a Bruker Avance III 600 MHz Ultrashielded Plus (Bruker BiosSpin GmbH, Rheinstetten, Germany) spectrometer equipped with a 5 mm QCI Cryoprobe, and with acquisition parameters listed in Table 3.2. ^{13}C MR spectra were processed using a line broadening of 1.0 Hz.

3.2.3 Preparation and acquisition of solution containing [5-^{13}C]L-glutamine

A sample containing [5-^{13}C]L-glutamine, diluted in D_2O (CDN isotopes, Pointe-Claire, Canada), was transferred to a high-quality 5 mm NMR tube. ^{13}C MR spectra were acquired using a Bruker Avance III 600 MHz Ultrashielded Plus (Bruker BiosSpin GmbH, Rheinstetten, Germany) spectrometer equipped with a 5 mm QCI Cryoprobe. Three MR spectra were acquired, one using a quantitative (Bruker: zgig) pulse program at 279 K and two using a non-quantitative pulse sequence (Bruker: zgpg30), where one MR spectrum was acquired at a temperature of 279 K and the other at 301.5 K. Information about method, spectrometer, pulse program, and acquisition parameters are listed in Table 3.3

Table 3.3: Method, spectrometer, pulse program and acquisition parameters for solution containing [5-^{13}C]L-glutamine.

	Quantitative	Non-quantitative
Method	^{13}C MRS	^{13}C MRS
Spectrometer	Bruker Avance III 600 MHz Ultrashielded Plus	Bruker Avance III 600 MHz Ultrashielded Plus
Pulse program	1D sequence with inverse gated decoupling zgig; Bruker	Single pulse with ^{1}H decoupling zgpg30; Bruker
Parameters:		
Spin rate	5 kHz	5 kHz
Flip angle	90°	30°
NS	256	2048
AQ	1.65 sec	1.65 sec
T_R	81.65 sec	2.15 sec
Sweep width	197 ppm/30 kHz	197 ppm/30 kHz
Temperature	279 K	279 K/301.5 K
Total time	6 h	1 h 15 min

MRS: magnetic resonance spectroscopy, NS: number of scans, AQ: acquisition time, T_R: repetition time.

3.3 Preprocessing and analysis of MRS metabolomics data

3.3.1 Preprocessing of MR spectra

MR spectra were preprocessed before analyzes by in-house made programs developed in MATLAB (The Mathworks, Inc.). **Baseline correction** was performed on all MR spectra (represented in Appendices C) using MATLAB R2017a (The MathWorks, Inc.). Baseline correction of MR spectra was performed by estimating the baseline for each MR spectra by using asymmetric least square [82]. Baselines of all ^{13}C MR spectra were in addition corrected for noise, where the mean amplitude of selected noise regions was found and subtracted from all data points in ^{13}C MR spectra. The resulting baselines of ^{13}C MR spectra then have noise varying around zero. **Peak alignment** of MR spectra was performed by icoshift [67] using MATLAB R2017a (The MathWorks, Inc.). **Normalization** was performed by normalizing MRS metabolomics data by using equal total area [65] or sample mass correction using the formula

$$X_{\mathrm{corr},i} = \frac{X_i \cdot \bar{m}}{m_i}$$

where $X_{\mathrm{corr},i}$ is the corrected MRS metabolomics data, X_i is the original MRS metabolomics data, $\bar{m}$ is the mean mass of all samples in a data set, and m_i is the mass of sample i (all sam-

ple masses are presented in appendices Table A.1). **Mean centering** was performed using PLS Toolbox 8.2.1 (Eigenvector Research, Inc.) in MATLAB R2017a (The MathWorks, Inc.). Table 3.4 summarize preprocessing methods performed on MRS metabolomics data before analyzes. L-glutamine(C5) at 180.4 ppm was used as an internal chemical shift reference for all ^{13}C MR spectra.

Table 3.4: Preprocessing methods performed on MRS metabolomics data prior to analysis.

	Baseline correction	Peak alignment	Normalization	Mean centering
Identification of ^{13}C-labeled metabolites	Asymmetric least square	icoshift	Sample mass correction	-
Integration of peaks from [5-^{13}C]L-glutamine	Asymmetric least square	-	-	-
Multivariate analysis	Asymmetric least square	icoshift	Equal total area	Yes
Amount of ^{13}C-labeled metabolites	Asymmetric least square	icoshift	Sample mass correction	-
Univariate analysis	Asymmetric least square	icoshift	Sample mass correction	-

3.3.2 Identification of metabolites in ^{13}C MR spectra originating from injected [5-^{13}C]L-glutamine

Identification of metabolites in ^{13}C MR spectra originating from [5-^{13}C]L-glutamine was carried out by calculating mean ^{13}C MR spectra from CB-839 treated, controls, and natural abundance MR spectra after ^{13}C MR spectra were preprocessed as described in Table 3.4. Mean ^{13}C MR spectra were found by calculating the mean value of each point in the ^{13}C MR spectra. Identification of metabolites was carried out by identifying the chemical shifts of peaks in the three mean ^{13}C MR spectra and comparing the values to chemical shifts found from the Human Metabolome Database (HMDB) [83] for metabolites expected to be found in the ^{13}C MR spectra. Metabolites originated from [5-^{13}C]L-glutamine were then identified by comparing the metabolites found in CB-839 treated and controls with the metabolites found in natural abundance mean ^{13}C MR spectrum. Metabolites found in only mean ^{13}C MR spectra of CB-839 treated and controls or with much higher signal than in the mean ^{13}C MR spectrum of natural abundance, were assumed to originated from the injected [5-^{13}C]L-glutamine.

3.3.3 ^{13}C-percentage of carbons on L-glutamine in [5-^{13}C]L-glutamine solution

A quantitative ^{13}C MR spectrum, of solution containing [5-^{13}C]L-glutamine, was preprocessed as described in Table 3.4 and integrated for each L-glutamine peak using MATLAB R2017a (The MathWorks, Inc.). The percentage of ^{13}C at each carbon position of L-glutamine was calculated by assuming that signal from carbon five on L-glutamine showed signal from 99 % of all L-glutamine in the solution, as listed in the product description. ^{13}C-percentages of L-glutamine(C1-C4), $p_{\mathrm{gln},i}$, were found by the formula

$$p_{\mathrm{gln},i} = \frac{\int X(\mathrm{C}i) \cdot 99\ \%}{\int X(\mathrm{C5})} \tag{4}$$

where $X(\mathrm{C}i)$ is the peak of L-glutamine at carbon position i in the ^{13}C MR spectrum and $X(\mathrm{C5})$ is the peak of L-glutamine at carbon position five in the ^{13}C MR spectrum.

3.3.4 Relative amount of ^{13}C-labeled metabolites

Relative amount of ^{13}C-labeled metabolites were found by integration of selected metabolite peaks in ^{13}C MR spectra using MATLAB R2017a (The MathWorks, Inc.) after preprocessing MR spectra as described in Table 3.4. CB-839 treated and control samples were compared by representing the integrals as box plots containing mean value, median value, and extreme values, using MATLAB R2017a (The MathWorks, Inc.).

3.3.5 Multivariate analyzes of MR spectra

Before multivariate analyzes were performed, MR spectra were preprocessed as described in Table 3.4, and areas with noise or unwanted signals, like the signal from water, were excluded before analyzing MR spectra. Included areas were 15 ppm-75 ppm and 173 ppm-185 ppm for ^{13}C MR spectra, and 0.5 ppm-4.8 ppm and 5.2 ppm-5.5 ppm for ^{1}H MR spectra.

PCA was performed on the preprocessed ^{1}H and ^{13}C MR spectra of tissue and ^{13}C MR spectra of serum from basal-like PDXs as described in Table 3.4. PCA was carried out using PLS Toolbox 8.2.1 (Eigenvector Research, Inc.) in MATLAB R2017a (The MathWorks, Inc.) and presented as score and loading plots for recommended PCs from PLS Toolbox 8.2.1 (Eigenvector Research, Inc.), which is based on percent variance captured by the PCA model. PLS-DA was performed on ^{1}H MR spectra of tissue, where a permutation test was performed to validate separation from random. The p-value of the permutation test was found from Equation (2).

3.3.6 Determination of outliers and univariate analyzes

Before performing univariate analyzes, MRS metabolomics data were preprocessed as described in Table 3.4, and selected metabolites, L-lactate(C1), L-glutamate(C5), and L-glutamine(C5), were integrated from ^{13}C MR spectra using MATLAB R2017a (The MathWorks, Inc.).

For extreme values, identified in box plots of integral values, a Dixon-type test was performed to determine if these data points were outliers. r_{10} values were calculated from Equation (3) and compared with the critical value found from Dixon [81]. If calculated r_{10} value of a data point was higher than the critical value, it was classified as an outlier and excluded before univariate analyzes were performed.

Univariate analyzes were performed on the integrals of selected peaks for both tissue and serum. A two-tailed Student's t-test was performed on the data fulfilling the requirement of normal distribution, using Excel 2013 (Microsoft), while a Wilcoxon rank sum test was performed, using Statistical Package for the Social Sciences (SPSS, IBM), if the data was not normally distributed. The degree of normalization was visually determined from Q-Q plots (represented in Appendix D), made by using SPSS (IBM) on the integral values of each of the selected metabolites in ^{13}C MR spectra. In the cases where it was doubt about the normal distribution, both tests were performed.

4 Results

4.1 Identification of metabolites in ^{13}C MR spectra

Metabolites were identified in mean ^{13}C MR spectra from basal-like PDX tissue from mice injected with [5-^{13}C]L-glutamine, one of CB-839 treated ($n = 6$) and one of controls ($n = 5$), see Figure 4.1 **A)** and **B)**. A third mean MR spectrum was of samples with only natural abundance of ^{13}C isotopes ($n = 3$), used to identify metabolites originating from injected [5-^{13}C]L-glutamine, see Figure 4.1 **C)**. Relevant metabolites identified from ^{13}C MR spectra are also listed in Table 4.1 together with chemical shifts of identified metabolites.

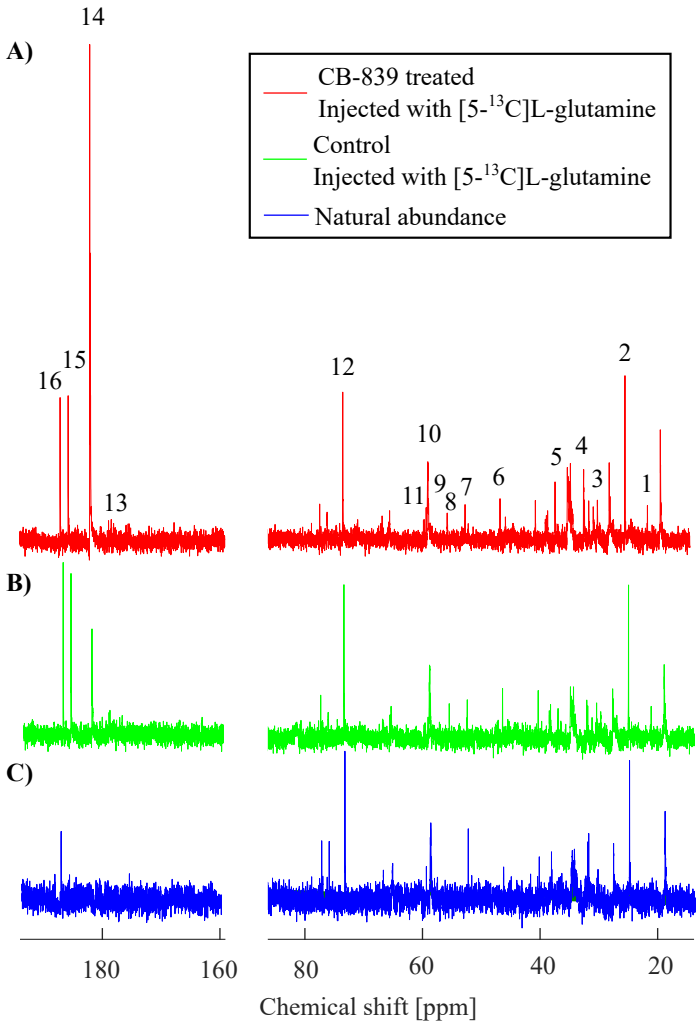

Figure 4.1: Representation of three mean ^{13}C MR spectra of tissue samples from basal-like patient-derived xenografts, with numbering of identified peaks. **A)** Mean ^{13}C MR spectrum of samples from mice treated with CB-839 ($n = 6$). **B)** Mean ^{13}C MR spectrum of samples from control mice ($n = 5$). **C)** Mean ^{13}C MR spectrum of mice with only natural abundance ($n = 3$). Each enumerated peak is listed in Table 4.1.

Table 4.1: List of the most important metabolites found in ^{13}C MR spectra of mice injected with [5-^{13}C]L-glutamine, with number for identification found in Figure 4.1 and identified chemical shifts. It is also listed if the signal from metabolites originated from the injected [5-^{13}C]L-glutamine.

Number in Figure 4.1	Metabolite (carbon no.)	Chemical shift ^{13}C [ppm]	Originates from injected [5-^{13}C]L-glutamine
1	L-alanine(C3)	19.0	Yes
2	L-lactate(C3)	22.8	
3	L-glutamine(C3)	29.0	
4	L-glutamate(C3)	29.8	
5	Glutathione(C4)	34.3	
6	L-glycine(C2)	44.3	
7	L-taurine	50.3	
8	L-alanine(C2)	53.3	Yes
9	Choline	56.6	
10	Phosphocholine	56.6	
11	Glycerophosphocholine	56.7	
12	L-lactate(C2)	71.2	
13	L-alanine(C1)	178.7	Yes
14	L-glutamine(C5)	180.4	Yes
15	L-glutamate(C5)	184.0	Yes
16	L-lactate(C1)	185.3	Yes

By comparing mean ^{13}C MR spectra in Figure 4.1, peaks originating from L-alanine(C1, C2, C3), L-glutamine(C5), L-glutamate(C5), and L-lactate(C1) were assumed to originate or partially originate from the injected [5-^{13}C]L-glutamine.

4.2 Signal from L-glutamine(C5) in ^{13}C MR spectra

^{13}C MR spectra of basal-like PDX tissue from mice injected with [5-^{13}C]L-glutamine showed four separated peaks for L-glutamine(C5) ($\sim$ 180.3 ppm). To investigate the origin of these peaks and to determine if all four peaks originated from L-glutamine, a solution containing [5-^{13}C]L-glutamine was analyzed by acquiring a ^{13}C MR spectrum with a quantitative MR pulse sequence, as shown in Figure 4.2 **A)**.

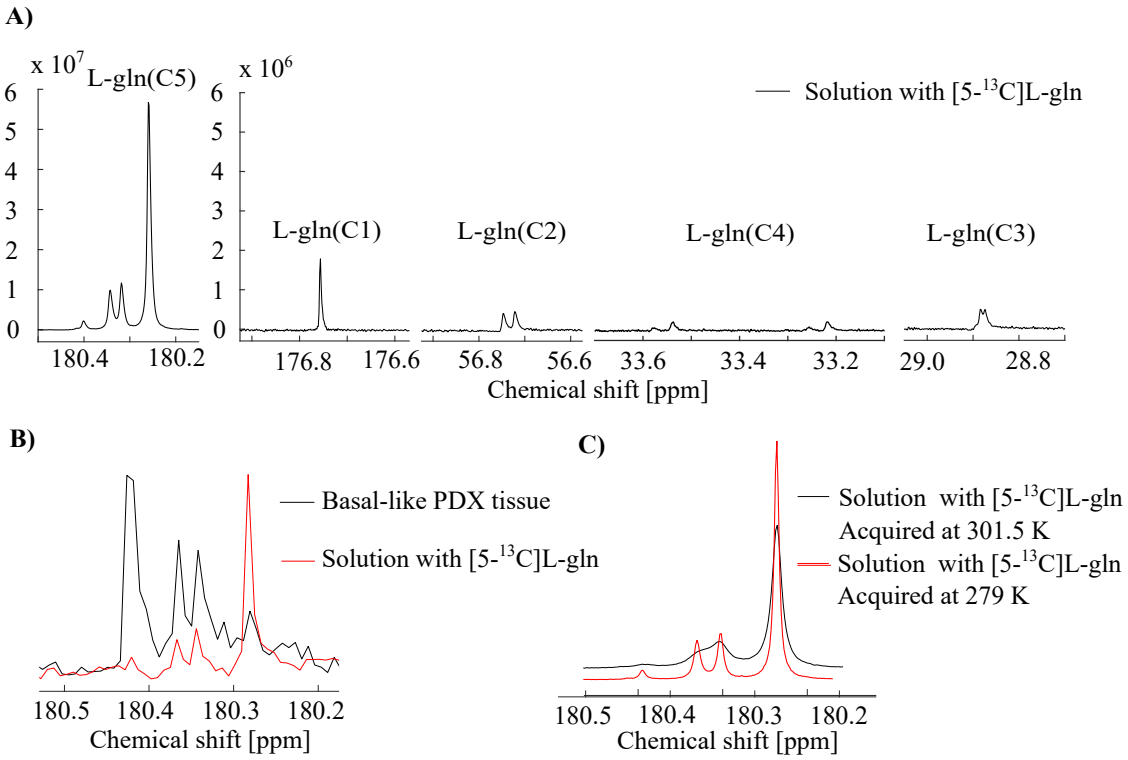

Figure 4.2: Representative ^{13}C MR spectra of L-glutamine in basal-like PDX tissue and solution containing [5-^{13}C]L-glutamine. **A)** A quantitative ^{13}C MR spectrum from [5-^{13}C]L-glutamine solution in all five carbon positions. **B)** ^{13}C MR spectra from basal-like PDX tissue and [5-^{13}C]L-glutamine solution from 180.2 ppm-180.5 ppm. **C)** ^{13}C MR spectra of [5-^{13}C]L-glutamine solution acquired at different temperatures, 301.5 K and 279 K. L-gln: L-glutamine, PDX: patient-derived xenograft.

From ^{13}C MR spectrum in Figure 4.2 **A)**, [5-^{13}C]L-glutamine solution showed signal from L-glutamine(C5) split into four peaks and also splitting of signal from L-glutamine(C2-C4). Integration of signal from different carbons in L-glutamine was calculated relatively to the integral of L-glutamine in position five (L-glutamine(C5)) by using Equation (4) to find the ^{13}C-percentage of L-glutamine(C1-C4). The results are represented in Table 4.2.

Table 4.2: ^{13}C-percentage of all carbons in L-glutamine found from a quantitative ^{13}C MR spectrum of [5-^{13}C]L-glutamine solution and the coupling pattern of each peak of L-glutamine in the ^{13}C MR spectrum.

L-gln carbon no.	^{13}C-percentage (%)	Coupling pattern
1	1.03	Singlet
2	1.02	Doublet
3	1.06	Partially split doublet
4	0.94	Two doublets
5	99	Split in four

Peaks around L-glutamine(C5) ($\sim$ 180.3 ppm) in two representative ^{13}C MR spectra, one from [5-^{13}C]L-glutamine solution and one from basal-like PDX tissue, were analyzed and are shown in Figure 4.2 **B)**. Both MR spectra contained four peaks with similar chemical shift change, but with different peak intensities. The ^{13}C MR spectrum from the basal-like PDX tumor tissue shows higher intensity at the peak with the highest chemical shift, while the ^{13}C MR spectrum of [5-^{13}C]L-glutamine solution shows higher intensity for the peak with the lowest chemical shift.

To better understand the origin of the splitting in the signal from L-glutamine(C5), a ^{13}C MR spectrum from solution with [5-^{13}C]L-glutamine acquired and analyzed at two different temperatures, 279 K and 301.5 K, shown in Figure 4.2 **C)**. The ^{13}C MR spectrum at 301.5 K shows broader signal peak with lower maximum intensity than the signal peak from the ^{13}C MR spectrum at 279 K, but with similar chemical shift between the peaks.

4.3 Integration and multivariate analyzes of MR spectra

4.3.1 Integration and PCA of ^{13}C MR spectra of basal-like PDX tissue

^{13}C MR spectra of basal-like PDX tissue from mice treated with CB-839 ($n = 6$) and controls ($n = 5$), were analyzed by integration and PCA (all integrals are represented in appendices Table B.1). Results of integration and PCA are represented in Figure 4.3.

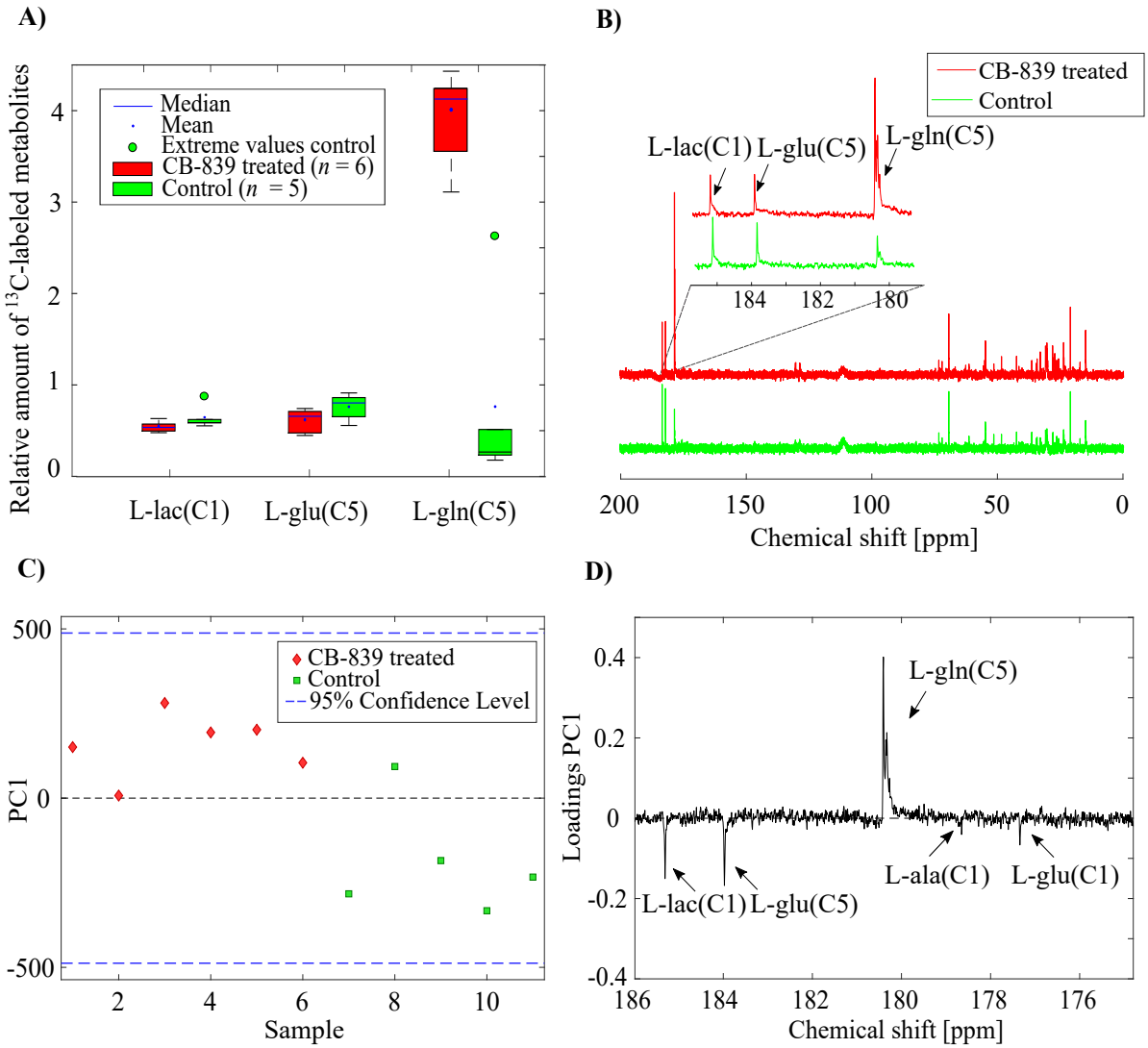

Figure 4.3: Results from analyzes of ^{13}C MR spectra of basal-like PDX tissue. **A)** Relative amount of L-lactate(C1), L-glutamate(C5), and L-glutamine(C5), found by integration of MR spectra, from CB-839 treated (red)($n = 6$) and controls (green)($n = 5$), represented in box plots. **B)** Mean ^{13}C MR spectra of CB-839 treated (red) and controls (green), with identified metabolites between 178 ppm and 184 ppm. **C)** Score plot from PCA of PC1, from samples of CB-839 treated (red) and controls (green), found by PCA, where PC1 explains 51.3 % of the variance in the data set. **D)** Loading plot for PC1 with identified metabolites. L-ala: L-alanine, L-gln: L-glutamine, L-glu: L-glutamate, L-lac: L-lactate.

Box plots in Figure 4.3 **A)** indicates that the levels of L-lactate(C1) and L-glutamate(C5) are not considerable different between CB-839 treated and controls, while the level of L-glutamine(C5) is higher in CB-839 treated than in controls. The box plots also show two extreme values, one in the control group of L-lactate(C1) and one in the control group

of L-glutamine(C5). Mean ^{13}C MR spectra of tumor samples from CB-839 treated and controls, in Figure 4.3 **B)**, shows the difference between L-lactate(C1), L-glutamate(C5), and L-glutamine(C5) in the two MR spectra and a higher level of L-glutamine(C5) is found in CB-839 treated than in controls and similar levels of L-lactate(C1) and L-glutamate(C1).

Score plot in Figure 4.3 **C)** from PCA of PC1 explains 51.3 % of the variance in the data set and shows that CB-839 treated and controls are separated, except from sample no. 8. CB-839 treated have a positive PC1 score, while controls have a negative PC1 score (except sample no. 8). For CB-839 treated with positive scores, the loading plot of PC1 in Figure 4.3 **D)**, shows a higher level of L-glutamine(C5) and lower levels of L-lactate(C1), L-glutamate(C5), L-alanine(C1), and L-glutamate(C1).

4.3.2 Integration and PCA of ^{13}C MR spectra of serum from mice with basal-like PDXs

^{13}C MR spectra acquired of serum samples from mice with basal-like PDXs were analyzed by integration and PCA (all integrals are represented in appendices Table B.2). The results of integration and PCA are represented in Figure 4.4.

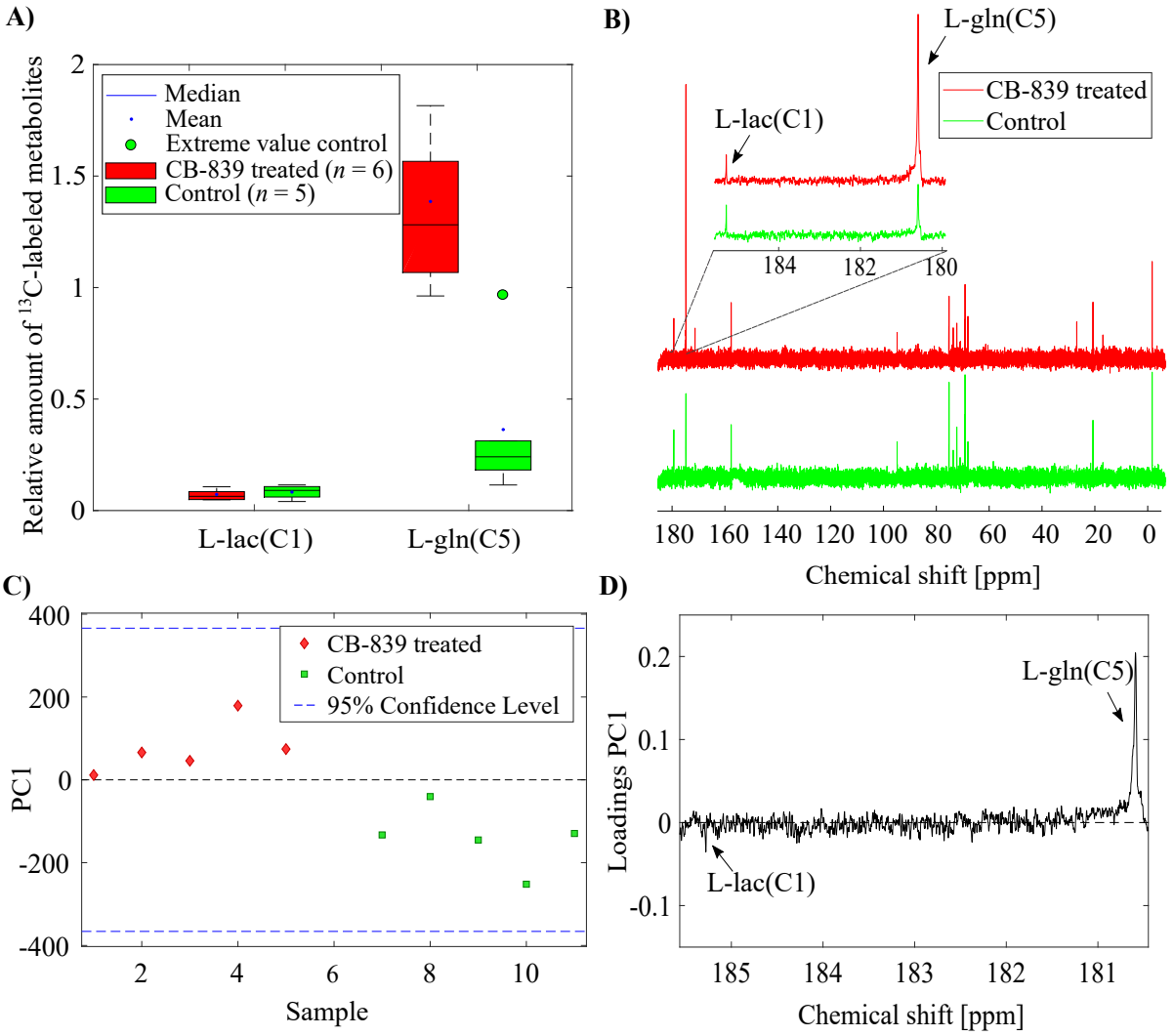

Figure 4.4: Results from analyzes of ^{13}C MR spectra of serum from mice with basal-like PDXs. **A)** Relative amount of L-lactate(C1) and L-glutamine(C5), found by integration, from CB-839 treated (red)($n = 6$) and controls (green)($n = 5$), represented as box plots. **B)** Mean ^{13}C MR spectra of serum samples from CB-839 treated (red) and controls (green), with identified metabolites from 180 ppm-186 ppm. **C)** Score plot from PCA of PC1 from tissue samples, of CB-839 treated (red) and controls (green), where PC1 explains 48.6 % of the variance in the data set. **D)** Loading plot for PC1 with ^{13}C-labeled metabolites. L-gln: L-glutamine, L-lac: L-lactate.

Box plots in Figure 4.4 **A)** indicates that the level of L-lactate(C1) in CB-839 treated and controls is not considerable different, but a higher level of L-glutamine(C5) in CB-839 treated than in controls is observed. The box plots also show one extreme value in the control group of L-glutamine(C5).

Mean ^{13}C MR spectra of serum from mice treated with CB-839 and controls, are represented in Figure 4.4 **B)** and shows the difference between L-lactate(C1) and L-glutamine(C5) in CB-839 treated and controls, with higher levels for L-glutamine(C5) in CB-839 treated and similar levels of L-lactate(C1).

Score plot from PCA of PC1 in Figure 4.4 **C)** explains 48.6 % of the variance in the data set and shows that CB-839 treated and controls are separated, where CB-839 treated have a positive PC1 score, while controls have a negative PC1 score. For CB-839 treated, with positive scores, the loading plot of PC1 in Figure 4.4 **D)** shows higher levels of L-glutamine(C5) and lower levels of L-lactate(C1).

4.3.3 PCA and PLS-DA of ^{1}H MR spectra of basal-like PDX tissue

^{1}H MR spectra of basal-like PDX tissue were analyzed by PCA and PLS-DA. Results from PCA are represented in Figure 4.5 and results from PLS-DA are represented in Figure 4.6.

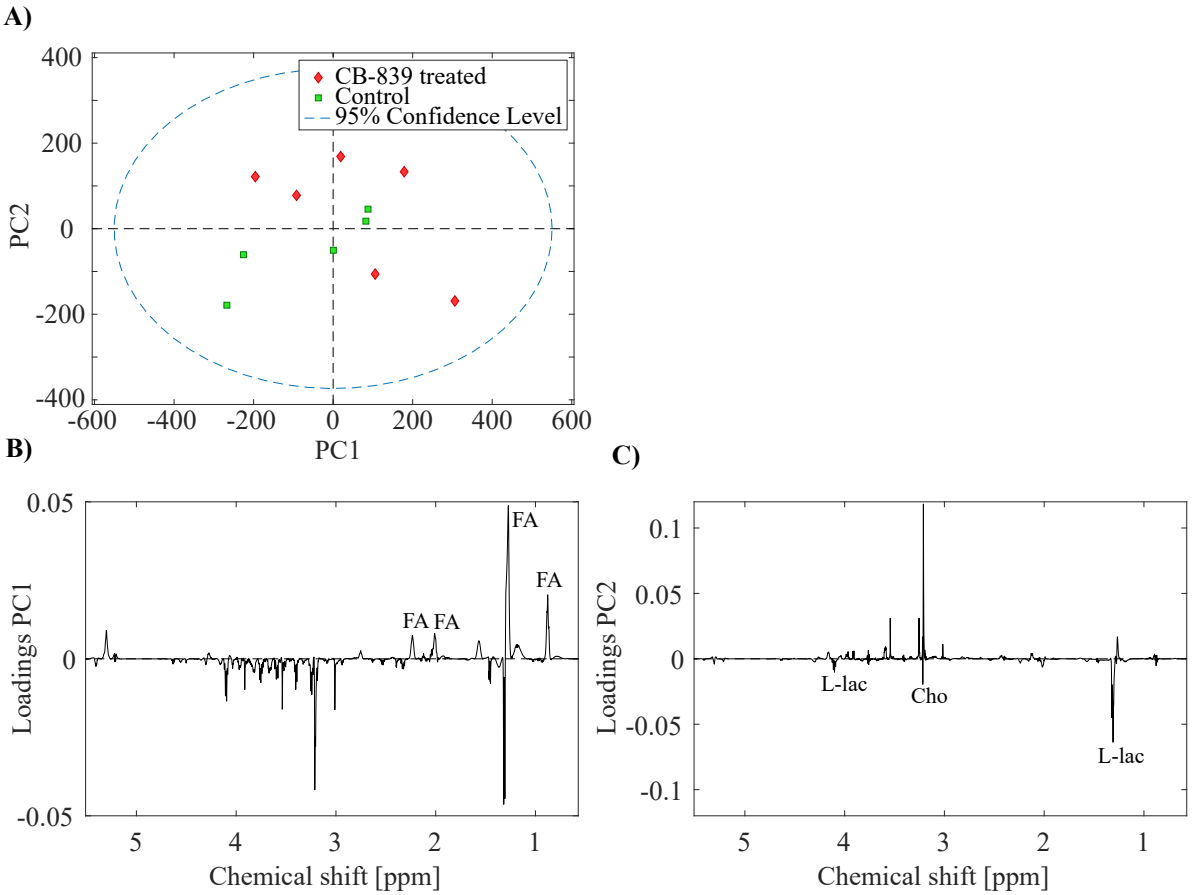

Figure 4.5: Results from PCA on ^{1}H MR spectra of the basal-like PDX tissue. **A)** Score plot from PCA of PC1 against PC2, where PC1 explained 57.2 % of the variance in the data set and PC2 26.3 %, of samples from CB-839 treated ($n = 6$) and controls ($n = 5$). **B)** Loading plot belonging to PC1 and **C)** Loading plot belonging to PC2. Cho: Choline, FA: fatty acids, L-lac: L-lactate.

The first two PC's found from PCA explained in total 83.5 % of the variance in the data set. From Figure 4.5 **A)** neither PC1 or PC2 shows any separation between the group coming from samples of mice treated with CB-839 and the control group treated with placebo. By looking at the loading plot for PC1 in Figure 4.5 **B)** it looks like the samples are separated between the samples with high concentrations of fat and those with lower concentrations of fat. From loading plot for PC2 in Figure 4.5 **C)** the separation seems to be divided into the samples with high and low concentrations of choline and L-lactate.

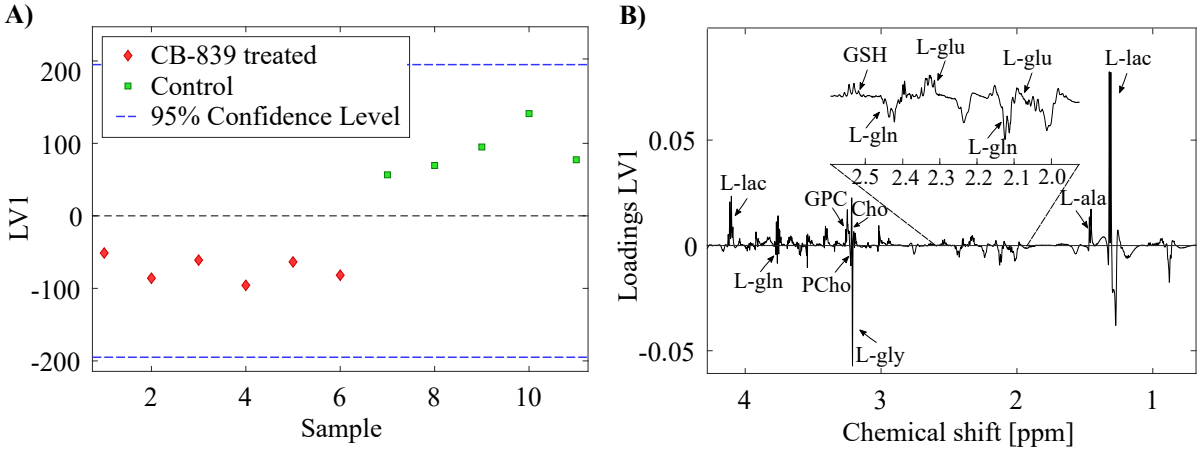

Figure 4.6: Representation of results from PLS-DA of ^{1}H MR spectra of basal-like PDX tissue from CB-839 treated (red)($n = 6$) and controls (green)($n = 5$). **A)** Score plot from PLS-DA of LV1, explaining 19.1 % of the variance in the data set, of samples from CB-839 treated and controls. **B)** Loading plot from PLS-DA of LV1 with identified metabolites. Cho: choline, GPC: glycerophosphocholine, GSH: glutathione, L-ala: L-alanine, L-gln: L-glutamine, L-glu: L-glutamate, L-gly: L-glycine.

Figure 4.6 **A)** shows the score plot from PLS-DA. The score plot from PLS-DA shows a clear separation between CB-839 treated and controls. Figure 4.6 **B)** shows the loading plot for LV1. For controls with positive scores, the loading plot shows higher levels of L-lactate, L-alanine, L-glutamate, glutathione, choline, and glycerophosphocholine and lower levels of L-glutamine, L-glycine, and phosphocholine. By performing a permutation test on the data, a p-value of 0.01 was found from Equation (2), making a statistical significant difference between the results found by PLS-DA and random.

4.4 Univariate analyzes of MRS metabolomics data

Univariate analyzes were performed on calculated integrals (see appendices Table B.1 for integrals of tissue and Table B.2 of serum) of selected ^{13}C-labeled metabolites from ^{13}C MR spectra of both tissue and serum samples from basal-like PDXs. Before univariate analyzes were performed, possible outliers were identified and eliminated. For the three extreme values found in box plots in Figure 4.3 **A)** and Figure 4.4 **A)**, a Dixon-type test was performed on the belonging integral values. r_{10} values were calculated from Equation (3) and were found to be 0.773 for L-lactate(C1) from sample no. 9 in tissue, 0.862 for L-glutamine(C5) from sample no. 8 in tissue, and 0.768 for L-glutamine(C5) from sample no. 8 in serum. The critical value for $n = 5$ samples, when a significance level of $\alpha = 0.05$ was chosen, is found from Dixon [81] to be 0.642, so all three extreme values classifies as being outliers and were excluded before performing univariate analyzes.

From Q-Q plots of selected metabolites, represented in Appendices D, normal distribution

of data sets was determined and a Student's t-test was chosen for normally distributed data sets, or else a Wilcoxon rank sum test was performed. The results of the tests are represented in Table 4.3.

Table 4.3: Representation of calculated p-values, from univariate analyzes, Student's t-test and Wilcoxon rank sum test, of integrals of selected peaks, L-lactate(C1), L-glutamate(C5), and L-glutamine(C5), from ^{13}C MR spectra between CB-839 treated and controls for both tissue and serum samples.

Sample type	Peak	Student's t-test (p-value)	Wilcoxon (p-value)
Tissue	L-lactate(C1)	0.25	-
Tissue	L-glutamate(C5)	0.13	-
Tissue	L-glutamine(C5)	$3.9 \cdot 10^{-7}$	0.010
Serum	L-lactate(C1)	0.56	0.537
Serum	L-glutamine(C5)	$1.9 \cdot 10^{-4}$	0.010

From Table 4.3 a significant difference, with a p-value ≤ 0.05, was observed between CB-839 treated and controls for L-glutamine(C5), using both Student's t-test and Wilcoxon rank sum test for integral values of both tissue and serum samples of basal-like PDXs. For L-lactate(C1) in both tissue and serum and L-glutamate(C5) in tissue, no significant difference between CB-839 treated and controls was found.

5 Discussion

5.1 Evaluation of PDX model, sample handling, and analytical methods

5.1.1 Evaluation of PDX model

The aim of this study was to investigate how basal-like/TN breast cancer responded to the drug CB-839 by using an *in vivo* PDX model. The goal for the model is to resemble human basal-like/TN breast cancer and predict drug response in the human body. PDX models have shown to reflect the heterogeneity of human tumors and maintain the genetic and morphological feature from the primary tumor [29, 30, 84, 85]. PDX models have also shown to give a good predictive value for clinical outcome [86], and can be good tools for investigating drug response in patients [30]. Still, there are some constraints using these models, where the main constraints involve the use of immunocompromised mice and the impact from a different microenvironment and stromal components in the mice [87]. PDX models will consequently not respond exactly as the human patient from which they originate, but can still be valuable models for response of cancer therapies [87]. In the PDX model used in this study, MAS98.12, both the model and the patient, from which the model originate from, were classified as basal-like and TN [11]. The tumors were orthotopically implanted into the mammary fat pad of the mice to get as similar microenvironment, histopathology, and gene expression as human basal-like/TN breast tumors [33]. MAS98.12 is consequently expected to give a valuable representation of human basal-like/TN breast cancer.

5.1.2 Evaluation of sample preparation

Preparation and acquisition of all samples were performed under similar conditions to get comparable MR spectra. To inhibit degradation of metabolites all samples were stored in liquid nitrogen until use, samples were prepared as fast as possible on a cooled block, and acquisition of MR spectra were performed at 277 K. Degradation will be limited as long as the samples are kept at low temperatures (273-275 K) [57]. To get comparable MR spectra, tissue samples were cut to pieces with similar sample mass and serum was mixed with the same amount of a lock reference in each sample. The color of the serum was clear yellow for most samples, but for some samples it was more red or pink, indicating that some of the red blood cells are analyzed. This may at least to some degree, influence the concentration of detected metabolites.

5.1.3 Evaluation of MRS acquisition

MR spectra from tumor tissue and serum samples from CB-839 treated and control mice were analyzed by ^{13}C MRS [12]. The drawback using ^{13}C MRS is the low sensitivity and accordingly a poor SNR in the MR spectra. This make contribution from noise high, which can interfere with the results when ^{13}C MR spectra are analyzed. Weak signals

from low-concentration metabolites may be mistakenly interpreted as noise and hence not detected. HR-MAS MRS was used to cancel out effects from dipole-dipole coupling and chemical shift anisotropy, which otherwise would increase the spectral line-widths in MR spectra [58]. In liquids, like serum, these effects are canceled out by molecular motion, and magic angle spinning is therefore not necessary [60]. ^{1}H MR spectra, which have a much higher sensitivity than ^{13}C MRS due to the higher natural abundance and a higher gyromagnetic ratio of ^{1}H, were also acquired for CB-839 treated and control samples to investigate low-concentration metabolites.

Equal acquisition parameters were used during MR acquisition. MR spectra were shimmed until formate achieved a FWHM of less than 1.5 Hz. Some variations of FWHM between the MR spectra were present, but the integral of peaks will remain the same. ^{13}C MR spectra acquired using a non-quantitative MR sequence, used a relatively short repetition time, T_R, compared to the relatively long T_1 relaxation of the carbonyl nuclei of L-glutamine(C5), L-glutamate(C5), and L-lactate(C1) [88, 89]. This will lead to weaker signal in the ^{13}C MR spectra from these nuclei due to less recovery of spins to the thermal equilibrium before a new rf pulse is added. Integrals from metabolites with different T_1 relaxation can for that reason not be compared in these MR spectra, but the same peak in different MR spectra will on the other hand have the same T_1. It can therefore be assumed that the same peak in different MR spectra, when using a non-quantitative pulse sequence, are comparable in this study.

5.1.4 Evaluation of MRS analyzes

Tumor tissue and serum samples from the basal-like PDX model were analyzed using ^{13}C MRS to investigate the metabolic pathway, glutaminolysis, during CB-839 treatment. By injecting [5-^{13}C]L-glutamine into mice, while still alive, it is possible to follow downstream metabolites from [5-^{13}C]L-glutamine. For analyzes of basal-like PDXs, metabolites originating from injected [5-^{13}C]L-glutamine were at interest. From ^{13}C MR spectra of basal-like PDX tissue, L-lactate(C1), L-glutamate(C1, C5), L-glutamine(C5), and L-alanine(C1, C2, C3) were identified as partly or fully originating from the injected [5-^{13}C]L-glutamine, from Figure 4.1. From these metabolites L-lactate(C1), L-glutamate(C5), L-glutamine(C5) were chosen for further analyzes because they are relevant for investigating how CB-839 effect metabolism of basal-like PDX tissue. Signal from L-alanine(C1, C2, C3) and L-glutamate(C1) were very low and just above the limit of detection. Integrals from these metabolites have consequently not been calculated. From ^{13}C MR spectra of serum, L-glutamate(C5) was not detected and analyzes were performed on L-lactate(C1) and L-glutamine(C5).

Evaluation of integration

As described in Section 5.1.2, samples preparation and acquisition were performed under similar conditions to get comparable MR spectra. Integrals from preprocessed ^{13}C MR spectra of tissue and serum were in addition scaled according to sample mass. The result-

ing integrals were therefore assumed to describe the amount of each metabolite taken up by the tumor tissue and in serum. The concentration of metabolites detected in serum is expected to be affected by the metabolism in the entire mouse, and not only the PDX tissue.

Evaluation of multivariate analyzes
The multivariate analysis PCA was performed on MR spectra to find explanations for variance between them. For PCs with separation between CB-839 treated and controls in score plot, the loading plot will show metabolites with high and low concentrations in the two groups. For MR spectra, where suggested PCs does not show any separation between the groups, there may be similar concentrations or small differences compared to other factors, like fat. To investigate if there still is a significant difference between the two groups a PLS-DA was performed, because it looks for variations between two predetermined groups [72]. To reassure that separation found by PLS-DA is better than random a leave one out permutation test was performed, where $p = 0.01$ is lower than the significance level and imply a significant separation between the results found by PLS-DA and random.

Evaluation of Dixon-type test and univariate analyzes
Outliers must be excluded before performing univariate analysis to keep the outliers from interfering with the mean value and the variance in the data sets [90]. For small samples sizes $n < 10$ a Dixon-type test is preferred as an outlier test because it does not require normal distribution and only look at the range between the data points [91].

Which univariate analysis best suited to analysis a data set depends on the data set properties. A Student's t-test requires that the data sets to be compared are normally distributed [77], because it uses the mean values from normally distribution data sets. On data sets with few samples and not normally distribution, a Wilcoxon rank sum test is often preferred [92], because it ranks data points and looks for classification and is therefore not dependent of the data set being normally distributed. The drawback with using a Wilcoxon rank sum compared to Student's t-test is loss of power, because the test does not take into consideration the degree of separation. For samples where it was uncertainty about normal distribution both tests were performed. Both tests showed, in all cases, the same results for significance and were assumed to be valid.

5.2 Evaluation of metabolites identified in ^{13}C MR spectra

Figure 2.2 shows the ^{13}C-labeling pattern from [5-^{13}C]L-glutamine and indicates which metabolites are expected to be found in ^{13}C MR spectra of tissue from mice injected with [5-^{13}C]L-glutamine. CB-839 inhibits the enzyme glutaminase which catalyzes the conversion from L-glutamine to L-glutamate [6, 48]. High concentrations of L-glutamine(C5) are consequently expected to be observed in CB-839 treated samples [6]. In addition, glutaminase inhibition may not be 100 % efficient. For this reason, one can also expect to find some other downstream metabolites of L-glutamine, including L-glutamate and metabolites in the TCA cycle in the CB-839 treated samples [39]. For control samples, the

conversion between L-glutamine and L-glutamate will be catalyzed by glutaminase. Lower concentrations of L-glutamine(C5) and higher concentrations of other metabolites in the glutaminolysis are consequently expected to be observed in these samples.

Carbon occurs naturally as ^{12}C (98.9 %), which is MR invisible with a spin $I = 0$, and as ^{13}C (1.1 %), which is MR visible with spin $I = \frac{1}{2}$. To determine which metabolites were present naturally in the basal-like/TN tumors, ^{13}C MR spectra from untreated ^{13}C-unlabeled tissue samples were compared with samples from mice injected with [5-^{13}C]L-glutamine, as shown in Figure 4.1. CB-839 treated and control samples contained the same metabolites, but with different concentrations. L-alanine(C1, C2, and C3) and L-glutamine(C5) were only identified in samples from mice injected with [5-^{13}C]L-glutamine and these metabolites can therefore be assumed to originate from the injected [5-^{13}C]L-glutamine. L-glutamate(C5) and L-lactate(C1) were found in both natural abundance and ^{13}C-labeled samples, but in much higher concentrations in the ^{13}C-labeled MR spectra. These metabolites can therefore also be assumed to originate from the injected [5-^{13}C]L-glutamine.

High levels of the injected [5-^{13}C]L-glutamine were taken up by the PDX tissue and converted into L-glutamate(C5), as shown in Figure 4.1. Relatively high levels of L-lactate(C1) were also found in ^{13}C MR spectra from ^{13}C-labeled compared to natural abundance tissue. L-lactate(C1) may originate from pyruvate and L-malate in the first turn of the TCA cycle [40]. Small concentrations of L-alanine(C1) were also observed in the ^{13}C-labeled MR spectra, and may also originate from pyruvate and L-malate in the first turn of the TCA cycle. The occurrence of ^{13}C-labeling on L-alanine(C2 and C3) are so far of unknown origin. Due to the low sensitivity of ^{13}C MRS, low-concentration metabolites are not detected. These metabolites can consequently not be separated from noise in the ^{13}C MR spectra.

5.3 Evaluation of signal from L-glutamine(C5) in ^{13}C MR spectra

^{13}C MR spectra were acquired using a proton decoupled pulse sequence and signal from each carbon atom in a molecule is therefore expected to appear as singlets, because the splitting due to proton decoupling is eliminated [93]. In ^{13}C MR spectra from basal-like PDX tissue, four peaks were identified around L-glutamine(C5) ($\sim$ 180.3 ppm). To clarify if all four peaks originated from the injected [5-^{13}C]L-glutamine, a quantitative ^{13}C MR spectrum was acquired of a solution containing [5-^{13}C]L-glutamine. The results, as shown in Figure 4.2 **A)**, confirms the assumption that all four peaks originate from L-glutamine, since the calculated ^{13}C-percentages of each peaks from L-glutamine(C1-C4) were approximately 1.1 %, which corresponds to the natural abundance of ^{13}C. The four peaks in ^{13}C MR spectrum of basal-like PDX tissue had also approximately the same chemical shifts as the solution containing [5- ^{13}C]L-glutamine, as represented in Figure 4.2 **B)**. This also indicates that all four peaks at $\sim$ 180.3 ppm in the ^{13}C MR spectra originates from L-glutamine(C5).

A possible explanation for the splitting of signal from L-glutamine is that L-glutamine

exists in different conformers [94, 95] in the samples, explained in Section 2.7.3, which gives a small change of the shielding of the carbon atoms in L-glutamine that can lead to detection of slightly different frequencies from L-glutamine. A change in shielding of a molecule will have larger change in chemical shift in a ^{13}C MR spectrum than in a ^{1}H MR spectrum, and it is therefore possible to detect splitting of the signal, due to different conformers, in ^{13}C MR spectra [55]. This explanation is valid if the change from one conformer to another is longer than the acquisition time of $\sim$ 1 sec for ^{13}C MRS [54].

From Figure 4.2 **B)**, there are signal intensity differences between the four peaks in the ^{13}C MR spectra of the basal-like PDX tumor sample and the [5-^{13}C]L-glutamine solution. If the splitting of L-glutamine is due to different conformers, the intensity differences will suggest that one conformer is more preferred in solution and another conformer is preferred in tissue. A possible reason for this effect is that L-glutamine can move more freely in solution than it can in tissue and that the preferred conformer of L-glutamine then changes [95, 96].

To better understand the mechanism behind the splitting of signal from L-glutamine two ^{13}C MR spectra were acquired of solution containing [5-^{13}C]L-glutamine at two different temperatures, 279 K and 301.5 K. The two ^{13}C MR spectra, in Figure 4.2 **C)**, shows that the peaks broadens when the temperature increases. The two middle peaks also fuse into one peak when the temperature increases. This supports the theory about the four peaks occur due to various of conformers of L-glutamine, because the peaks behave like a fast-chemical exchange of conformers in the ^{13}C MR spectra, which is expected when the temperature increases [54].

5.4 Evaluation of metabolic response of CB-839 in basal-like PDXs

^{13}C MRS analyzes of CB-839 treated and control MAS98.12 tumors show that these tumors contained ^{13}C-labeled metabolites, indicating that the tumors take up L-glutamine and convert L-glutamine into other metabolites including L-glutamate and L-lactate. Even more importantly, CB-839 treated samples had significantly higher concentrations of L-glutamine than controls, which strongly suggests that CB-839 inhibits conversion from L-glutamine to L-glutamate in these tumors [6]. Since CB-839, given as a single agent, does not inhibit growth of MAS98.12 tumors (as shown in appendices Figure E.1), these results indicate that the MAS98.12 tumors are not dependent on L-glutamine to maintain tumor growth and cell proliferation. These tumors must consequently use other pathways than glutaminolysis to maintain the rate of tumor growth. Glycolysis is a natural pathway to consider, but a previous study on MAS98.12 showed decreased glycolytic activity in MAS98.12 tumors compared to another luminal like model [12], indicating that these tumors uses alternative pathways to maintain tumor growth.

Slightly higher concentrations of L-lactate(C1) and L-glutamate(C5) were observed in con-

trol compared to CB-839 treated samples, but the differences were not statistical significant. If assuming that the total amount of other downstream metabolites is small, the results indicates that the total amount of ^{13}C-labeled metabolites is lower in control tumor samples compared to CB-839 treated samples. If this is true, it could mean that CB-839 is affecting the uptake of L-glutamine into the tumor. Another possible explanation is that L-glutamate, L-lactate, or other downstream metabolites are pumped out of the cells [8, 97], or a third possible scenario, that L-glutamine is converted into many other metabolites with too weak signal to be detected in ^{13}C MR spectra.

Serum from the tumor-bearing mice were analyzed by ^{13}C MRS to investigate how much L-glutamine was present in the serum, and to study if other ^{13}C-labeled metabolites were released from the tumor or other tissues into the bloodstream. Similarly, as for PDX tissue, significant higher levels of L-glutamine were found in serum from CB-839 treated than in control mice. Higher concentrations of L-glutamine observed in the CB-839 treated mice may be caused by an increased release of L-glutamine from other organs of the mice, caused by CB-839. Another explanation is that CB-839 treated mice have a lower uptake of the injected [5-^{13}C]L-glutamine from the bloodstream due to higher concentrations of L-glutamine in the tumor tissue. Gross [6] has shown that CB-839 inhibits consumption of L-glutamine into cancer cells *in vitro*. Since glutaminase is expressed in several organs of the mice, including kidney and brain, it is likely that L-glutamine consumption from the bloodstream into these organs is reduced [6]. In addition, in mice bearing subcutaneous TNBC tumors an increase in concentration of L-glutamine was found in CB-839 treated tumors (CTG-0052) and serum compared with controls tumor and serum samples. The tumor growth was also reduced when these tumors were treated with CB-839 [6]. In another basal-like, HER2 positive xenograft model JIMT1, CB-839 inhibited tumor growth both as a single agent and in combination with paclitaxel [6]. No signal from ^{13}C-labeled L-glutamate was detected in serum, but ^{13}C-labeled L-lactate was observed in both CB-839 treated and controls, with similar concentrations between the two groups. These results indicate that ^{13}C-labeled metabolites released from tumor tissue will not end up in the bloodstream, and are most likely taken up by nearby tissue or organs in the mouse or that ^{13}C-labeled metabolites have distributed into many other metabolites in small undetectable amounts.

A possible explanation of where ^{13}C-labeled metabolites in controls end up is pumping of L-lactate and L-glutamate from cancer cells into the extracellular domain. Cancer cells are known for pumping L-lactate out of the cell and into the extracellular domain, and are also found to release L-glutamate into the extracellular domain through L-glutamate/L-cystine antiporters, x_c^- [8, 42, 43, 98]. When inside the cell, L-cystine is converted into L-cysteine and is used to synthesize glutathione together with L-glycine and L-glutamate. This is consistence with results found in Figure 4.6, showing higher concentrations of glutathione in ^{1}H MR spectra of basal-like PDX tissue and lower concentrations of L-glycine. From the discussion above, suggested metabolic pathways of L-glutamine in CB-839 treated cells are shown in Figure 5.1 **A)** and in control cell shown in Figure 5.1 **B)**. It is not possible to

know if signals detected in MR spectra originate from inside the cells or in the intermediate space between the cells, so if L-glutamate remain in the extracellular domain it would still be detected by ^{13}C MRS.

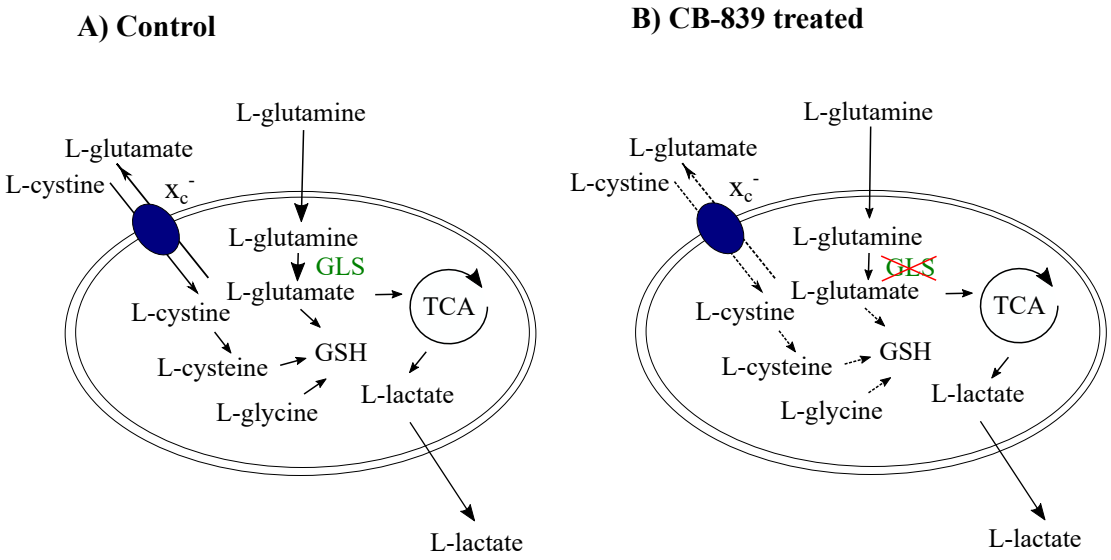

Figure 5.1: Suggested metabolic pathways of L-glutamine in basal-like MAS98.12 cells. **A)** Suggested metabolic pathway for control cells. L-glutamine enters the cell and is converted into L-glutamate catalyzed by glutaminase. L-glutamate can enter the TCA cycle, where L-lactate is produced and pumped out of the cell, or L-glutamate pumped out of the cell while L-cystine is pumped in by the L-glutamate/L-cystine antiporter, x_c^-, and converted into L-cysteine, or L-glutamate is used for production of glutathione together with L-cysteine and L-glycine. **B)** Suggested metabolic pathway of L-glutamine in CB-839 treated cells. L-glutamine enters the cell and is to some degree converted into L-glutamate. L-glutamate goes into the TCA cycle, where L-lactate is produced and pumped out of the cell. L-glutamate may also to some degree be pumped out of the cell through x_c^- and produce glutathione. GLS: glutaminase, GSH: glutathione, TCA: tricarboxylic acid cycle.

All things considered, it seems like some basal-like/TN models are dependent on L-glutamine [6] while others, like MAS98.12, are not. The effect of CB-839 is currently being investigated in early stage clinical trials of TNBC patients (Calithera Biosciences, Inc.) [10]. Preliminary results from phase I show that, among 23 TNBC patients receiving CB-839 in combination with paclitaxel 31 % had a partial response while 69 % of the patients showed response or stable disease [10]. CB-839 does not inhibit tumor growth in all patients, at least not as a single agent, but a better understanding of the metabolic phenotype

associated with response and resistance may help identifying the responders and the non-responders. One of the main advantage of this study was the possibility of directly tracing ^{13}C-labeled L-glutamine under treatment of CB-839. In future ^{13}C preclinical studies, it would be interesting to study the effect of CB-839 in combination with other therapies like paclitaxel or radiation. It would also be relevant to investigate the uptake and conversion of L-glutamine in nearby tissue and organs. Another possible study could be to measure glycolytic activity during CB-839 treatment.

6 Conclusion

The aim of this study was to add more information about the metabolic response in basal-like MAS98.12 tumors when treated with CB-839. Understanding the metabolic response to CB-839 in basal-like PDXs could help predicting the response of CB-839 in basal-like breast cancer patients.

From mice injected with [5-^{13}C]L-glutamine, significantly higher levels of L-glutamine were found in MAS98.12 tumors treated with CB-839 compared with controls. This imply that CB-839 inhibits the conversion from L-glutamine to L-glutamate, causing L-glutamine to accumulate in tumor. No significant increase in concentration of ^{13}C-labeled metabolites, like L-glutamate, L-lactate, or other downstream metabolites, were found in samples from CB-839 treated compared with controls. This may be explained by downstream metabolites from L-glutamine being released from tumor tissue or production of metabolites in small concentrations not detectable by ^{13}C MRS. Since CB-839 does not inhibit tumor growth in MAS98.12 tumors the results indicate that these tumors can get supply of essential nutrients, for cell proliferation and tumor growth, from other sources than L-glutamine. From analyzes of serum samples, significantly higher levels of L-glutamine were found in CB-839 treated compared with controls. This suggests that CB-839 leads to a decrease in the overall uptake of L-glutamine from the bloodstream to other organs and tissue of the mouse.

Together these results indicate that the basal-like PDX model MAS98.12 is not dependent on supply of L-glutamine for tumor growth. In future studies, other basal-like/TNBC PDX models should be investigates and metabolism in basal-like/TNBC tumors should also be further investigated to find additional sources, supporting tumor growth in addition to L-glutamine, to see if CB-839 can be combined with other treatments to enhance the treatment outcome.

References

[1] E Senkus, S Kyriakides, S Ohno, F Penault-Llorca, P Poortmans, E Rutgers, Sophia Zackrisson, and F Cardoso. Primary breast cancer: Esmo clinical practice guidelines for diagnosis, treatment and follow-up. *Annals of oncology*, 26(suppl 5):v8–v30, 2015.

[2] Philippe Autier, Mathieu Boniol, Carlo LaVecchia, Lars Vatten, Anna Gavin, Clarisse Héry, and Mary Heanue. Disparities in breast cancer mortality trends between 30 european countries: retrospective trend analysis of who mortality database. *Bmj*, 341:c3620, 2010.

[3] David R Wise and Craig B Thompson. Glutamine addiction: a new therapeutic target in cancer. *Trends in biochemical sciences*, 35(8):427–433, 2010.

[4] Ralph J DeBerardinis, Anthony Mancuso, Evgueni Daikhin, Ilana Nissim, Marc Yudkoff, Suzanne Wehrli, and Craig B Thompson. Beyond aerobic glycolysis: transformed cells can engage in glutamine metabolism that exceeds the requirement for protein and nucleotide synthesis. *Proceedings of the National Academy of Sciences*, 104(49):19345–19350, 2007.

[5] Alexandre Cassago, Amanda PS Ferreira, Igor M Ferreira, Camila Fornezari, Emerson RM Gomes, Kai Su Greene, Humberto M Pereira, Richard C Garratt, Sandra MG Dias, and Andre LB Ambrosio. Mitochondrial localization and structure-based phosphate activation mechanism of glutaminase c with implications for cancer metabolism. *Proceedings of the National Academy of Sciences*, 109(4):1092–1097, 2012.

[6] Matt I Gross, Susan D Demo, Jennifer B Dennison, Lijing Chen, Tania Chernov-Rogan, Bindu Goyal, Julie R Janes, Guy J Laidig, Evan R Lewis, Jim Li, et al. Antitumor activity of the glutaminase inhibitor cb-839 in triple-negative breast cancer. *Molecular cancer therapeutics*, 13(4):890–901, 2014.

[7] Hélène Pelicano, Wan Zhang, Jinyun Liu, Naima Hammoudi, Jiale Dai, Rui-Hua Xu, Lajos Pusztai, and Peng Huang. Mitochondrial dysfunction in some triple-negative breast cancer cell lines: role of mtor pathway and therapeutic potential. *Breast cancer research*, 16(5):434, 2014.

[8] Luika A Timmerman, Thomas Holton, Mariia Yuneva, Raymond J Louie, Mercè Padró, Anneleen Daemen, Min Hu, Denise A Chan, Stephen P Ethier, Laura J van't Veer, et al. Glutamine sensitivity analysis identifies the xct antiporter as a common triple-negative breast tumor therapeutic target. *Cancer cell*, 24(4):450–465, 2013.

[9] AM DeMichele, JJ Harding, ML Telli, P Münster, RR McKay, O Iliopoulos, S Whiting, KW Orford, MK Bennett, JW Mier, et al. Abstract p6-11-05: Phase 1 study of cb-839, a small molecule inhibitor of glutaminase (gls), in combination with paclitaxel (pac) in patients (its) with triple negative breast cancer (tnbc), 2017.

[10] Calithera Bioscience. Calithera biosciences reports cb-839 phase i triple negative breast cancer combination data at the 2016 san antonio breast cancer symposium,. http://ir.calithera.com/phoenix.zhtml?c=253557&p=RssLanding&cat=news&id=2227919, 2016. Accessed June 8, 2017.

[11] Anna Bergamaschi, Geir Olav Hjortland, Tiziana Triulzi, Therese Sørlie, Hilde Johnsen, Anne Hansen Ree, Hege Giercksky Russnes, Sigurd Tronnes, Gunhild M Mælandsmo, Oystein Fodstad, et al. Molecular profiling and characterization of luminal-like and basal-like in vivo breast cancer xenograft models. *Molecular oncology*, 3(5-6):469–482, 2009.

[12] Maria T Grinde, Siver A Moestue, Eldrid Borgan, Øystein Risa, Olav Engebraaten, and Ingrid S Gribbestad. 13c high-resolution-magic angle spinning mrs reveals differences in glucose metabolism between two breast cancer xenograft models with different gene expression patterns. *NMR in Biomedicine*, 24(10):1243–1252, 2011.

[13] Douglas Hanahan and Robert A Weinberg. Hallmarks of cancer: the next generation. *cell*, 144(5):646–674, 2011.

[14] Douglas Hanahan and Robert A Weinberg. The hallmarks of cancer. *cell*, 100(1):57–70, 2000.

[15] SJ Yeung, J Pan, and M-H Lee. Roles of p53, myc and hif-1 in regulating glycolysis—the seventh hallmark of cancer. *Cellular and Molecular Life Sciences*, 65(24):3981–3999, 2008.

[16] Jacques Ferlay, Isabelle Soerjomataram, Rajesh Dikshit, Sultan Eser, Colin Mathers, Marise Rebelo, Donald Maxwell Parkin, David Forman, and Freddie Bray. Cancer incidence and mortality worldwide: sources, methods and major patterns in globocan 2012. *International journal of cancer*, 136(5):E359–E386, 2015.

[17] Harald Weedon-Fekjær, Kjersti Bakken, Lars J Vatten, and Steinar Tretli. Understanding recent trends in incidence of invasive breast cancer in norway: age-period-cohort analysis based on registry data on mammography screening and hormone treatment use. *BMJ*, 344:e299, 2012.

[18] Jorge S Reis-Filho and Lajos Pusztai. Gene expression profiling in breast cancer: classification, prognostication, and prediction. *The Lancet*, 378(9805):1812–1823, 2011.

[19] Charles M Perou, Therese Sørlie, Michael B Eisen, Matt van de Rijn, Stefanie S Jeffrey, Christian A Rees, Jonathan R Pollack, Douglas T Ross, Hilde Johnsen, Lars A Akslen, et al. Molecular portraits of human breast tumours. *Nature*, 406(6797):747–752, 2000.

[20] Therese Sørlie, Robert Tibshirani, Joel Parker, Trevor Hastie, James Stephen Marron, Andrew Nobel, Shibing Deng, Hilde Johnsen, Robert Pesich, Stephanie Geisler, et al. Repeated observation of breast tumor subtypes in independent gene expression data sets. *Proceedings of the National Academy of Sciences*, 100(14):8418–8423, 2003.

[21] Therese Sørlie, Charles M Perou, Robert Tibshirani, Turid Aas, Stephanie Geisler, Hilde Johnsen, Trevor Hastie, Michael B Eisen, Matt Van De Rijn, Stefanie S Jeffrey, et al. Gene expression patterns of breast carcinomas distinguish tumor subclasses with clinical implications. *Proceedings of the National Academy of Sciences*, 98(19):10869–10874, 2001.

[22] Darina Vuong, Peter T Simpson, Benjamin Green, Margaret C Cummings, and Sunil R Lakhani. Molecular classification of breast cancer. *Virchows Archiv*, 465(1):1–14, 2014.

[23] Bernard Fisher, Carol Redmond, Edwin R Fisher, and Richard Caplan. Relative worth of estrogen or progesterone receptor and pathologic characteristics of differentiation as indicators of prognosis in node negative breast cancer patients: findings from national surgical adjuvant breast and bowel project protocol b-06. *Journal of Clinical Oncology*, 6(7):1076–1087, 1988.

[24] François Bertucci, Pascal Finetti, Nathalie Cervera, Benjamin Esterni, Fabienne Hermitte, Patrice Viens, and Daniel Birnbaum. How basal are triple-negative breast cancers? *International journal of Cancer*, 123(1):236–240, 2008.

[25] Katrina R Bauer, Monica Brown, Rosemary D Cress, Carol A Parise, and Vincent Caggiano. Descriptive analysis of estrogen receptor (er)-negative, progesterone receptor (pr)-negative, and her2-negative invasive breast cancer, the so-called triple-negative phenotype. *Cancer*, 109(9):1721–1728, 2007.

[26] Leslie H Sobin and Irvin D Fleming. Tnm classification of malignant tumors, (1997). *Cancer*, 80(9):1803–1804, 1997.

[27] Mary Cianfrocca and Lori J Goldstein. Prognostic and predictive factors in early-stage breast cancer. *The oncologist*, 9(6):606–616, 2004.

[28] Franco Lumachi, Davide A Santeufemia, and Stefano MM Basso. Current medical treatment of estrogen receptor-positive breast cancer. *World journal of biological chemistry*, 6(3):231, 2015.

[29] Yoko S DeRose, Guoying Wang, Yi-Chun Lin, Philip S Bernard, Saundra S Buys, Mark TW Ebbert, Rachel Factor, Cindy Matsen, Brett A Milash, Edward Nelson, et al. Tumor grafts derived from women with breast cancer authentically reflect tumor pathology, growth, metastasis and disease outcomes. *Nature medicine*, 17(11):1514–1520, 2011.

[30] Elisabetta Marangoni, Anne Vincent-Salomon, Nathalie Auger, Armelle Degeorges, Franck Assayag, Patricia de Cremoux, Ludmilla De Plater, Charlotte Guyader, Gonzague De Pinieux, Jean-Gabriel Judde, et al. A new model of patient tumor-derived breast cancer xenografts for preclinical assays. *Clinical Cancer Research*, 13(13):3989–3998, 2007.

[31] Xiumei Zhao, Zhigang Liu, Litian Yu, Yujing Zhang, Patricia Baxter, Horatiu Voicu, Sivashankarappa Gurusiddappa, Joseph Luan, Jack M Su, Hon-chiu Eastwood Leung, et al. Global gene expression profiling confirms the molecular fidelity of primary tumor-based orthotopic xenograft mouse models of medulloblastoma. *Neuro-oncology*, 14(5):574–583, 2012.

[32] Despina Siolas and Gregory J Hannon. Patient-derived tumor xenografts: transforming clinical samples into mouse models. *Cancer research*, 73(17):5315–5319, 2013.

[33] Michael P Kim, Douglas B Evans, Huamin Wang, James L Abbruzzese, Jason B Fleming, and Gary E Gallick. Generation of orthotopic and heterotopic human pancreatic cancer xenografts in immunodeficient mice. *Nature protocols*, 4(11):1670–1680, 2009.

[34] B Rubio-Viqueira and M Hidalgo. Direct in vivo xenograft tumor model for predicting chemotherapeutic drug response in cancer patients. *Clinical Pharmacology & Therapeutics*, 85(2), 2009.

[35] David L Nelson, Albert L Lehninger, and Michael M Cox. *Lehninger principles of biochemistry*. Macmillan, 2008.

[36] Jason W Locasale and Lewis C Cantley. Altered metabolism in cancer. *Bmc Biology*, 8(1):88, 2010.

[37] Harry Eagle, Vance I Oyama, Mina Levy, Clara L Horton, Ralph Fleischman, et al. The growth response of mammalian cells in tissue culture to l-glutamine and l-glutamic acid. *Journal of Biological Chemistry*, 218:607–616, 1956.

[38] Lawrence J Reitzer, Burton M Wice, and David Kennell. Evidence that glutamine, not sugar, is the major energy source for cultured hela cells. *Journal of Biological Chemistry*, 254(8):2669–2676, 1979.

[39] JM Mates, JA Segura, M Martin-Rufian, JA Campos-Sandoval, FJ Alonso, and J Marquez. Glutaminase isoenzymes as key regulators in metabolic and oxidative stress against cancer. *Current molecular medicine*, 13(4):514–534, 2013.

[40] RW Moreadith, , and AL Lehninger. The pathways of glutamate and glutamine oxidation by tumor cell mitochondria. role of mitochondrial nad (p)+-dependent malic enzyme. *Journal of Biological Chemistry*, 259(10):6215–6221, 1984.

[41] Brian J Altman, Zachary E Stine, and Chi V Dang. From krebs to clinic: glutamine metabolism to cancer therapy. *Nature Reviews Cancer*, 2016.

[42] Mohit K Sharma, Eric P Seidlitz, and Gurmit Singh. Cancer cells release glutamate via the cystine/glutamate antiporter. *Biochemical and biophysical research communications*, 391(1):91–95, 2010.

[43] Cynthia L Collins, Masafumi Wasa, Wiley W Souba, and Steve F Abcouwer. Determinants of glutamine dependence and utilization by normal and tumor-derived breast cell lines. *Journal of cellular physiology*, 176(1):166–178, 1998.

[44] Alton Meister. Glutathione deficiency produced by inhibition of its synthesis, and its reversal; applications in research and therapy. *Pharmacology & therapeutics*, 51(2):155–194, 1991.

[45] Isaac Marin-Valencia, Chendong Yang, Tomoyuki Mashimo, Steve Cho, Hyeonman Baek, Xiao-Li Yang, Kartik N Rajagopalan, Melissa Maddie, Vamsidhara Vemireddy, Zhenze Zhao, et al. Analysis of tumor metabolism reveals mitochondrial glucose oxidation in genetically diverse human glioblastomas in the mouse brain in vivo. *Cell metabolism*, 15(6):827–837, 2012.

[46] L Jin, GN Alesi, and S Kang. Glutaminolysis as a target for cancer therapy. *Oncogene*, 2015.

[47] Byron DeLaBarre, Jonathan Hurov, Giovanni Cianchetta, Stuart Murray, and Lenny Dang. Action at a distance: allostery and the development of drugs to target cancer cell metabolism. *Chemistry & biology*, 21(9):1143–1161, 2014.

[48] Jian-Bin Wang, Jon W Erickson, Reina Fuji, Sekar Ramachandran, Ping Gao, Ramani Dinavahi, Kristin F Wilson, Andre LB Ambrosio, Sandra MG Dias, Chi V Dang, et al. Targeting mitochondrial glutaminase activity inhibits oncogenic transformation. *Cancer cell*, 18(3):207–219, 2010.

[49] Jim Li, Lijing Chen, Bindu Goyal, Guy Laidig, Timothy Friend Stanton, and Eric Brian Sjogren. Heterocyclic inhibitors of glutaminase, December 10 2013. US Patent 8,604,016.

[50] Jim Pipe. Pulse sequences for diffusion-weighted mri. *Diffusion MRI: from quantitative measurement to in-vivo neuroanatomy. Academic Press, Amsterdam Boston*, pages 11–35, 2009.

[51] Joseph B Lambert and Eugene P Mazzola. *Nuclear magnetic resonance spectroscopy: an introduction to principles, applications, and experimental methods.* Pearson education, 2004.

[52] Nicolaas Bloembergen, Edward Mills Purcell, and Robert V Pound. Relaxation effects in nuclear magnetic resonance absorption. *Physical review*, 73(7):679, 1948.

[53] HS Gutowsky and A Saika. Dissociation, chemical exchange, and the proton magnetic resonance in some aqueous electrolytes. *The Journal of Chemical Physics*, 21(10):1688–1694, 1953.

[54] Oscar Millet, J Patrick Loria, Christopher D Kroenke, Miquel Pons, and Arthur G Palmer. The static magnetic field dependence of chemical exchange linebroadening defines the nmr chemical shift time scale. *Journal of the American Chemical Society*, 122(12):2867–2877, 2000.

[55] Hideji Fujiwara, Ajay K Bose, Maghar S Manhas, and James M van der Veen. 13 c nuclear magnetic resonance studies on the conformation of substituted hydantoins. *Journal of the Chemical Society, Perkin Transactions 2*, (11):1573–1577, 1980.

[56] Aliya Qayyum. Mr spectroscopy of the liver: Principles and clinical applications 1. *Radiographics*, 29(6):1653–1664, 2009.

[57] Beathe Sitter, Ursula Sonnewald, Manfred Spraul, Hans E Fjösne, and Ingrid S Gribbestad. High-resolution magic angle spinning mrs of breast cancer tissue. *NMR in Biomedicine*, 15(5):327–337, 2002.

[58] Tone F Bathen, Beathe Sitter, Torill E Sjøbakk, May-Britt Tessem, and Ingrid S Gribbestad. Magnetic resonance metabolomics of intact tissue: a biotechnological tool in cancer diagnostics and treatment evaluation. *Cancer research*, 70(17):6692–6696, 2010.

[59] Jacek W Hennel and Jacek Klinowski. Magic-angle spinning: a historical perspective. In *New techniques in solid-state nmr*, pages 1–14. Springer, 2005.

[60] LL Cheng, MJ Ma, L Becerra, T Ptak, I Tracey, A Lackner, and RG Gonzalez. Quantitative neuropathology by high resolution magic angle spinning proton magnetic resonance spectroscopy. *Proceedings of the National Academy of Sciences*, 94(12):6408–6413, 1997.

[61] ER Andrew, A Bradbury, and RG Eades. Removal of dipolar broadening of nuclear magnetic resonance spectra of solids by specimen rotation. 1959.

[62] JL Griffin and O Corcoran. High-resolution magic-angle spinning 13c nmr spectroscopy of cerebral tissue. *Magnetic Resonance Materials in Physics, Biology and Medicine*, 18(1):51–56, 2005.

[63] Ryan T Mckay. How the 1d-noesy suppresses solvent signal in metabonomics nmr spectroscopy: An examination of the pulse sequence components and evolution. *Concepts in Magnetic Resonance Part A*, 38(5):197–220, 2011.

[64] Teodor Perella. Pulse program catalogue: I. 1d & 2d nmr experiments. Bruker Biospin, Barcelona, 2006.

[65] Leslie R Euceda, Guro F Giskeødegård, and Tone F Bathen. Preprocessing of nmr metabolomics data. *Scandinavian journal of clinical and laboratory investigation*, 75(3):193–203, 2015.

[66] Tim De Meyer, Davy Sinnaeve, Bjorn Van Gasse, Ernst-R Rietzschel, Marc L De Buyzere, Michel R Langlois, Sofie Bekaert, José C Martins, and Wim Van Criekinge. Evaluation of standard and advanced preprocessing methods for the univariate analysis of blood serum 1h-nmr spectra. *Analytical and bioanalytical chemistry*, 398(4):1781–1790, 2010.

[67] Francesco Savorani, Giorgio Tomasi, and Søren Balling Engelsen. icoshift: A versatile tool for the rapid alignment of 1d nmr spectra. *Journal of Magnetic Resonance*, 202(2):190–202, 2010.

[68] Agnieszka Smolinska, Lionel Blanchet, Lutgarde MC Buydens, and Sybren S Wijmenga. Nmr and pattern recognition methods in metabolomics: from data acquisition to biomarker discovery: a review. *Analytica chimica acta*, 750:82–97, 2012.

[69] Andrew Craig, Olivier Cloarec, Elaine Holmes, Jeremy K Nicholson, and John C Lindon. Scaling and normalization effects in nmr spectroscopic metabonomic data sets. *Analytical chemistry*, 78(7):2262–2267, 2006.

[70] Michel J Anzanello, Rafael S Ortiz, Renata Limberger, and Kristiane Mariotti. Performance of some supervised and unsupervised multivariate techniques for grouping authentic and unauthentic viagra and cialis. *Egyptian Journal of Forensic Sciences*, 4(3):83–89, 2014.

[71] Svante Wold, Kim Esbensen, and Paul Geladi. Principal component analysis. *Chemometrics and intelligent laboratory systems*, 2(1-3):37–52, 1987.

[72] Z Ramadan, D Jacobs, M Grigorov, and S Kochhar. Metabolic profiling using principal component analysis, discriminant partial least squares, and genetic algorithms. *Talanta*, 68(5):1683–1691, 2006.

[73] CL Gavaghan, ID Wilson, and JK Nicholson. Physiological variation in metabolic phenotyping and functional genomic studies: use of orthogonal signal correction and pls-da. *FEBS letters*, 530(1-3):191–196, 2002.

[74] Johan A Westerhuis, Huub CJ Hoefsloot, Suzanne Smit, Daniel J Vis, Age K Smilde, Ewoud JJ van Velzen, John PM van Duijnhoven, and Ferdi A van Dorsten. Assessment of plsda cross validation. *Metabolomics*, 4(1):81–89, 2008.

[75] Hyune-Ju Kim, Michael P Fay, Eric J Feuer, Douglas N Midthune, et al. Permutation tests for joinpoint regression with applications to cancer rates. *Statistics in medicine*, 19(3):335–351, 2000.

[76] Winston Haynes. Student's t-test. In *Encyclopedia of Systems Biology*, pages 2023–2025. Springer, 2013.

[77] Joost CF de Winter. Using the student's t-test with extremely small sample sizes. *Practical Assessment, Research & Evaluation*, 18(10):1–12, 2013.

[78] Bernard Rosner. *Fundamentals of biostatistics*. Nelson Education, 2015.

[79] Frank Wilcoxon. Individual comparisons by ranking methods. *Biometrics bulletin*, 1(6):80–83, 1945.

[80] Asghar Ghasemi, Saleh Zahediasl, et al. Normality tests for statistical analysis: a guide for non-statisticians. *International journal of endocrinology and metabolism*, 10(2):486–489, 2012.

[81] Wilfred J Dixon. Analysis of extreme values. *The Annals of Mathematical Statistics*, 21(4):488–506, 1950.

[82] Paul H C Eilers and Brian D Marx. Generalized linear additive smooth structures. *Journal of Computational and Graphical Statistics*, 11(4):758–783, 2002.

[83] David S Wishart, Timothy Jewison, An Chi Guo, Michael Wilson, Craig Knox, Yifeng Liu, Yannick Djoumbou, Rupasri Mandal, Farid Aziat, Edison Dong, et al. Hmdb 3.0—the human metabolome database in 2013. *Nucleic acids research*, page gks1065, 2012.

[84] Monique D Topp, Lynne Hartley, Michele Cook, Valerie Heong, Emma Boehm, Lauren McShane, Jan Pyman, Orla McNally, Sumitra Ananda, Marisol Harrell, et al. Molecular correlates of platinum response in human high-grade serous ovarian cancer patient-derived xenografts. *Molecular oncology*, 8(3):656–668, 2014.

[85] Manoel Nunes, Patricia Vrignaud, Sophie Vacher, Sophie Richon, Astrid Lièvre, Wulfran Cacheux, Louis-Bastien Weiswald, Gerald Massonnet, Sophie Chateau-Joubert, André Nicolas, et al. Evaluating patient-derived colorectal cancer xenografts as preclinical models by comparison with patient clinical data. *Cancer research*, 75(8):1560–1566, 2015.

[86] JI Johnson, S Decker, D Zaharevitz, LV Rubinstein, JM Venditti, S Schepartz, S Kalyandrug, M Christian, S Arbuck, M Hollingshead, et al. Relationships between drug activity in nci preclinical in vitro and in vivo models and early clinical trials. *British journal of cancer*, 84(10):1424, 2001.

[87] James R Whittle, Michael T Lewis, Geoffrey J Lindeman, and Jane E Visvader. Patient-derived xenograft models of breast cancer and their predictive power. *Breast cancer research*, 17(1):17, 2015.

[88] Ferdia A Gallagher, Mikko I Kettunen, Sam E Day, De-en Hu, Magnus Karlsson, Anna Gisselsson, Mathilde H Lerche, and Kevin M Brindle. Detection of tumor glutamate metabolism in vivo using 13c magnetic resonance spectroscopy and hyperpolarized [1-13c] glutamate. *Magnetic resonance in medicine*, 66(1):18–23, 2011.

[89] Sam E Day, Mikko I Kettunen, Ferdia A Gallagher, De-En Hu, Mathilde Lerche, Jan Wolber, Klaes Golman, Jan Henrik Ardenkjaer-Larsen, and Kevin M Brindle. Detecting tumor response to treatment using hyperpolarized 13c magnetic resonance imaging and spectroscopy. *Nature medicine*, 13(11):1382, 2007.

[90] Edward H Livingston. Who was student and why do we care so much about his t-test? 1. *Journal of Surgical Research*, 118(1):58–65, 2004.

[91] Steven Walfish. A review of statistical outlier methods. *Pharmaceutical technology*, 30(11):82, 2006.

[92] Patrick D Bridge and Shlomo S Sawilowsky. Increasing physicians' awareness of the impact of statistics on research outcomes: comparative power of the t-test and wilcoxon rank-sum test in small samples applied research. *Journal of clinical epidemiology*, 52(3):229–235, 1999.

[93] R Freeman, HDW Hill, and R Kaptein. Proton-decoupled nmr. spectra of carbon-13 with the nuclear overhauser effect suppressed. *Journal of Magnetic Resonance (1969)*, 7(3):327–329, 1972.

[94] Simon C Lovell, J Michael Word, Jane S Richardson, and David C Richardson. Asparagine and glutamine rotamers: B-factor cutoff and correction of amide flips yield distinct clustering. *Proceedings of the National Academy of Sciences*, 96(2):400–405, 1999.

[95] Christian X Weichenberger and Manfred J Sippl. Self-consistent assignment of asparagine and glutamine amide rotamers in protein crystal structures. *Structure*, 14(6):967–972, 2006.

[96] Logan S Ahlstrom, Ivan I Vorontsov, Jun Shi, and Osamu Miyashita. Effect of the crystal environment on side-chain conformational dynamics in cyanovirin-n investigated through crystal and solution molecular dynamics simulations. *PloS one*, 12(1):e0170337, 2017.

[97] Gregg L Semenza. Tumor metabolism: cancer cells give and take lactate. *The Journal of clinical investigation*, 118(12):3835–3837, 2008.

[98] Eric P Seidlitz, Mohit K Sharma, Zeina Saikali, Michelle Ghert, and Gurmit Singh. Cancer cell lines release glutamate into the extracellular environment. *Clinical & experimental metastasis*, 26(7):781–787, 2009.

Appendices

A Additional information about samples and MR acquisition

Additional information about basal-like PDX tissue samples and acquisition parameters are listed in Table A.1.

Table A.1: Sample mass of all eleven tissue samples together with information about which mice were treated with CB-839, mice mass, and FWHM of formate after shimming.

Mouse no.	Treated with CB-839	Mice mass (g)	Sample mass (mg)	Shimming FWHM (Hz)
1	Yes	27.8	39.9	0.7
2	Yes	32.0	29.2	0.7
3	Yes	26.5	37.6	1.3
4	Yes	26.5	38.2	1.1
5	Yes	27.7	37.7	1.4
6	Yes	29.4	39.0	0.9
7	No	24.7	34.1	1.4
8	No	29.5	42.8	2.5
9	No	26.3	33.8	1.9
10	No	29.7	40.4	1.0
11	No	26.3	36.4	1.1

B Integrals of metabolites in ^{13}C MR spectra

Calculated integrals of L-lactate(C1), L-glutamate(C5), and L-glutamine(C5) in ^{13}C MR spectra of basal-like PDX tissue are listed in Table B.1 and of L-lactate(C1) and L-glutamine(C5) in serum in Table B.2. Calculation of integrals were performed using MATLAB R2017a (The Mathworks, Inc.).

Table B.1: Integral of L-lactate(C1), L-glutamate(C5), and L-glutamine(C5) from ^{13}C MR spectra (see Appendices C for ^{13}C MR spectra) of basal-like PDX tissue injected with [5-^{13}C]L-glutamine.

Mouse	L-lactate(C1)	L-glutamate(C5)	L-glutamine(C5)
1	5904323	7613056	42239701
2	4084967	4743943	24424854
3	6391139	4522595	41280108
4	5281239	7300341	45517408
5	4845639	5094433	42284333
6	6229558	7781574	45219640
7	5068822	7897566	1625728
8	6743502	7509665	30028992
9	7782172	7298598	4659913
10	6754995	9913740	2528357
11	5749955	5447025	2604200

Table B.2: Integral of L-lactate(C1) and L-glutamine(C5) in ^{13}C MR spectra (see Appendices C for ^{13}C MR spectra) of serum from basal-like PDXs injected with [5-^{13}C]L-glutamine.

Mouse nr.	L-lactate(1)	L-glutamine(5)
1	1065669	9623367
2	499438	12328255
3	1007013	11728042
4	479980	18022969
5	586629	13302167
6	683355	18160040
7	1146197	2408288
8	1071898	9660033
9	603787	1817625
10	402235	1144473
11	901091	3121583

C MR spectra

MR spectra acquired using Topspin 3.5 (Bruker), baseline corrected and plotted using MATLAB R2017a (The MathWorks, Inc.). For details about sample mass of the samples analyzed in the different MR spectra, see Table A.1. ^{13}C MR spectra are not regulated for L-glutamine(C5) at 180.4 ppm, so L-glutamine(C5) is found at $\sim$ 178.6 ppm.

C.1 ^{13}C MR spectra from basal-like PDXs treated with CB-839

^{13}C MR spectra from basal-like PDXs of mice treated with CB-839.

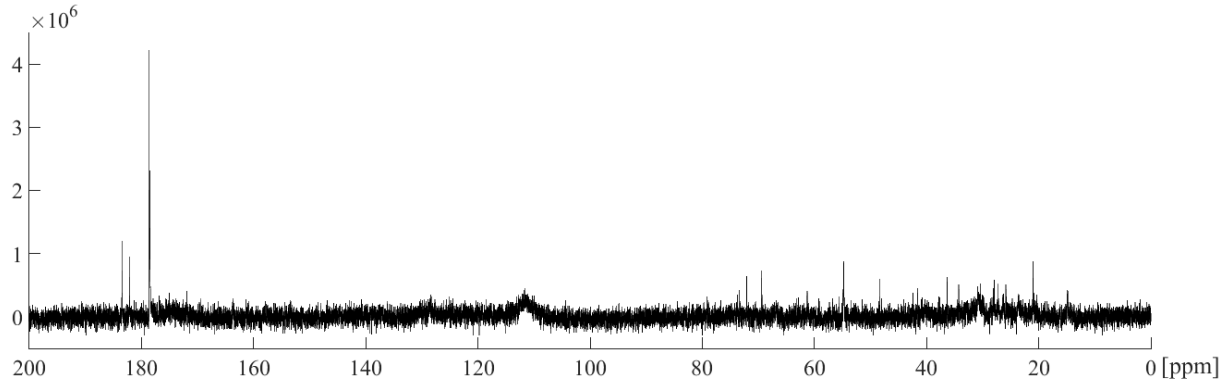

Figure C.1: ^{13}C HR-MAS MR spectrum of basal-like PDX tissue from mouse no. 1, treated with CB-839.

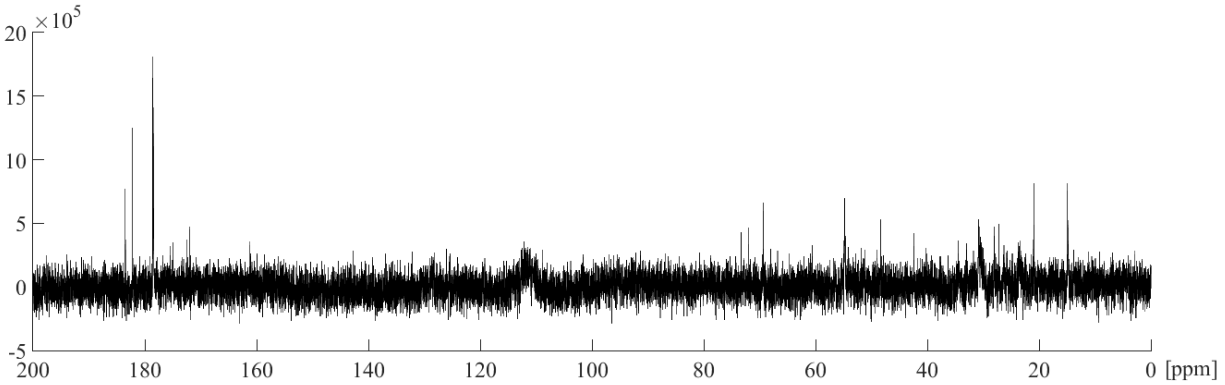

Figure C.2: ^{13}C HR-MAS MR spectrum of basal-like PDX tissue from mouse no. 2, treated with CB-839.

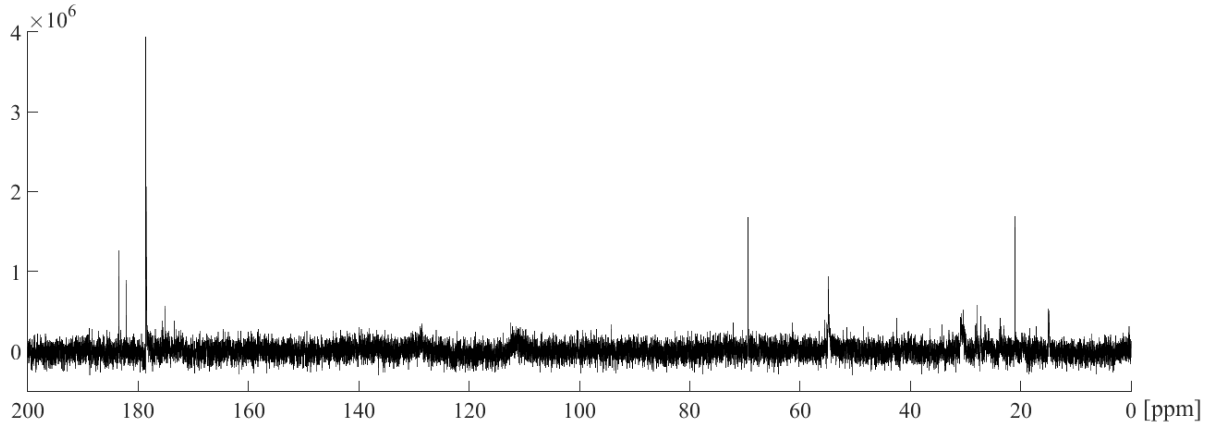

Figure C.3: ^{13}C HR-MAS MR spectrum of basal-like PDX tissue from mouse no. 3, treated with CB-839.

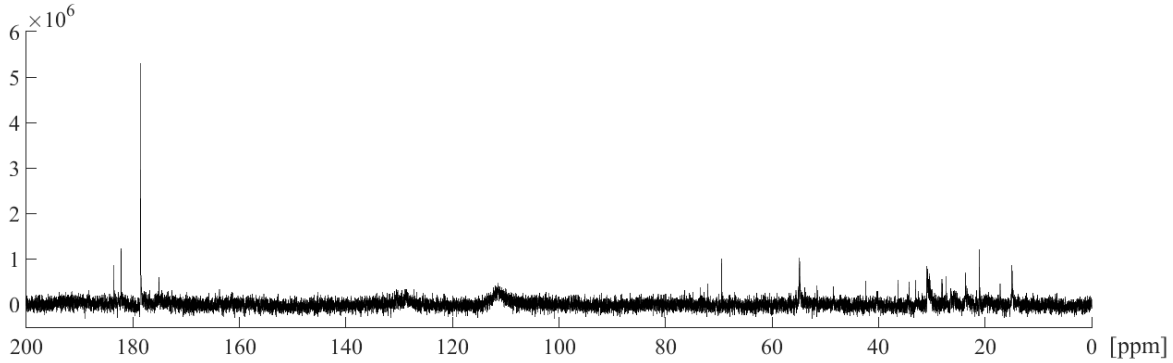

Figure C.4: ^{13}C HR-MAS MR spectrum of basal-like PDX tissue from mouse no. 4, treated with CB-839.

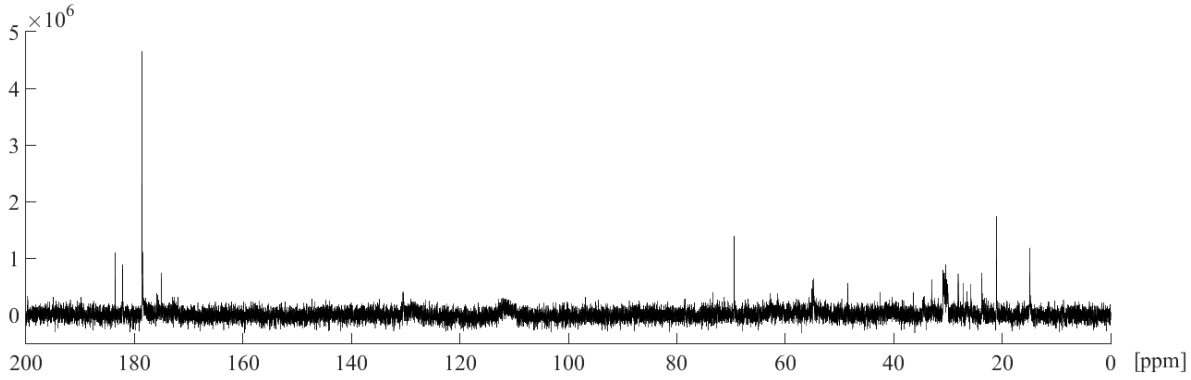

Figure C.5: ^{13}C HR-MAS MR spectrum of basal-like PDX tissue from mouse no. 5, treated with CB-839.

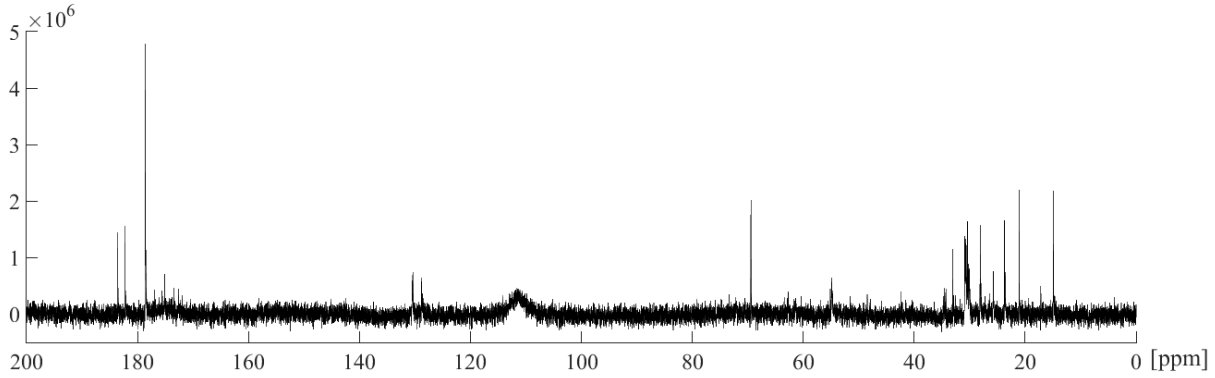

Figure C.6: ^{13}C HR-MAS MR spectrum of basal-like PDX tissue from mouse no. 6, treated with CB-839.

C.2 ^{13}C MR spectra from controls of basal-like PDX tissue

^{13}C MR spectra of basal-like PDX tissue from untreated control mice.

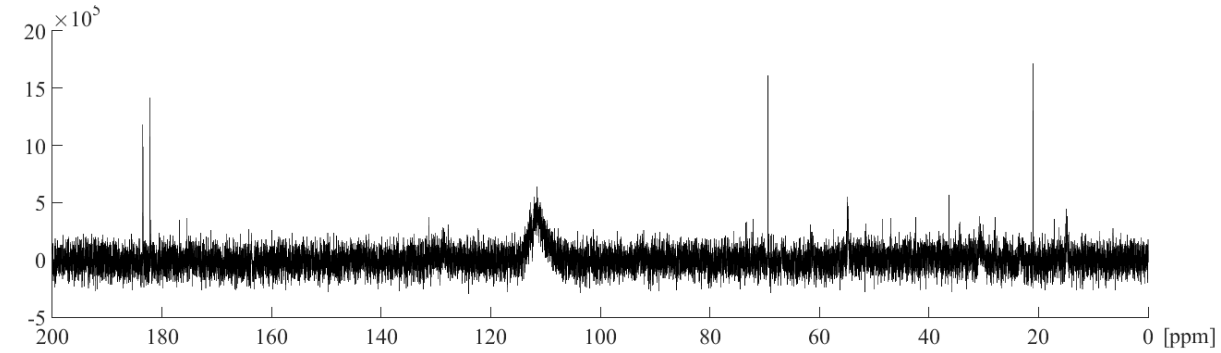

Figure C.7: ^{13}C HR-MAS MR spectrum of basal-like PDX tissue from control mouse no. 7.

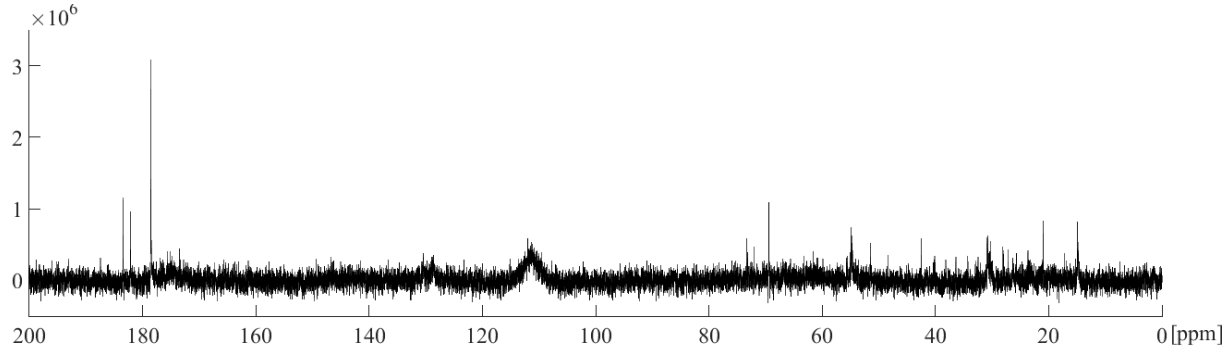

Figure C.8: ^{13}C HR-MAS MR spectrum of basal-like PDX tissue from control mouse no. 8.

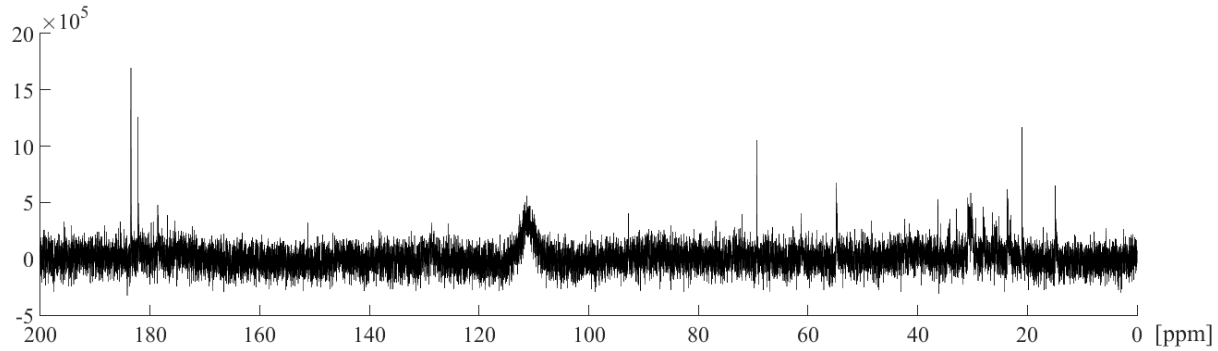

Figure C.9: ^{13}C HR-MAS MR spectrum of basal-like PDX tissue from control mouse no. 9.

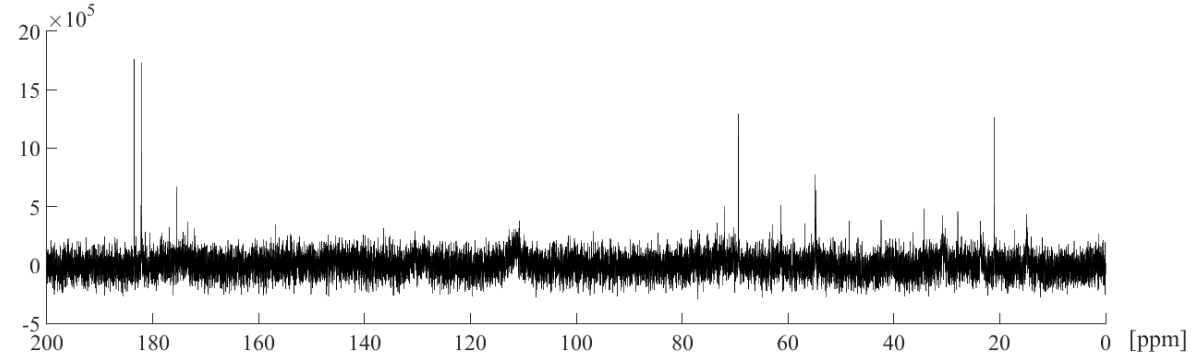

Figure C.10: ^{13}C HR-MAS MR spectrum of basal-like PDX tissue from control mouse no. 10.

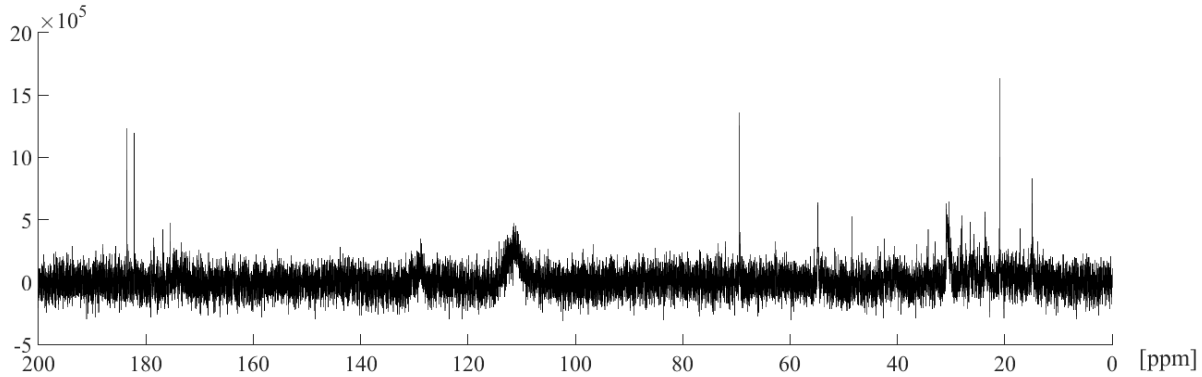

Figure C.11: ^{13}C HR-MAS MR spectrum of basal-like PDX tissue from control mouse no. 11.

C.3 ^{1}H MR spectra from basal-like PDX tissue treated with CB-839

^{1}H MR spectra from basal-like PDX tissue of mice treated with CB-839.

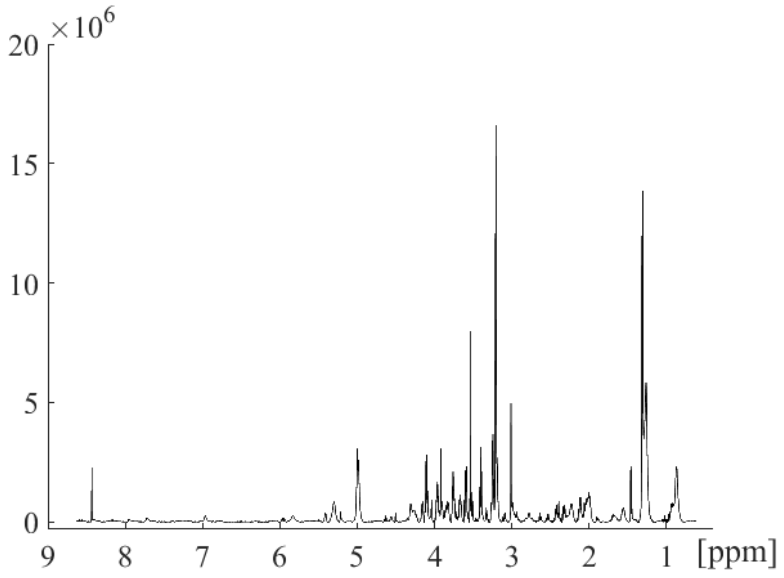

Figure C.12: ^{1}H HR-MAS MR spectrum of basal-like PDX tissue from CB-839 treated mouse no. 1.

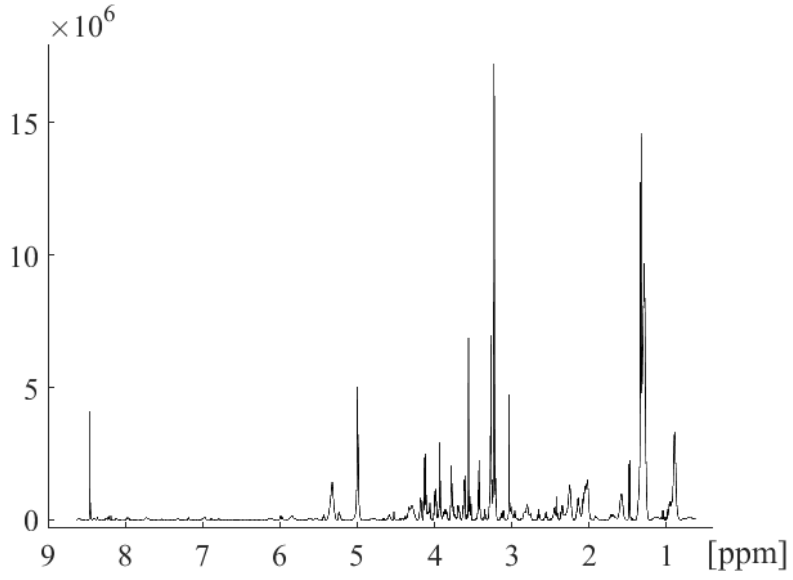

Figure C.13: ^{1}H HR-MAS MR spectrum of basal-like PDX tissue from CB-839 treated mouse no. 2.

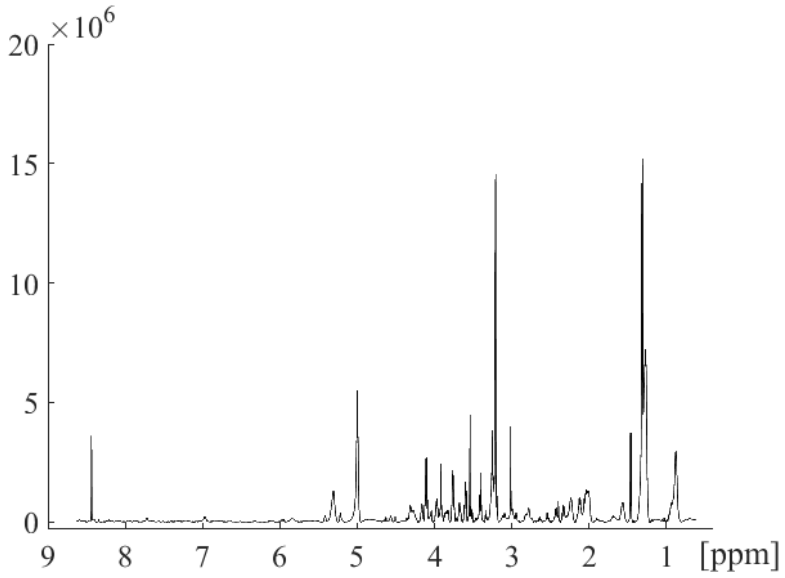

Figure C.14: ^{1}H HR-MAS MR spectrum of basal-like PDX tissue from CB-839 treated mouse no. 3.

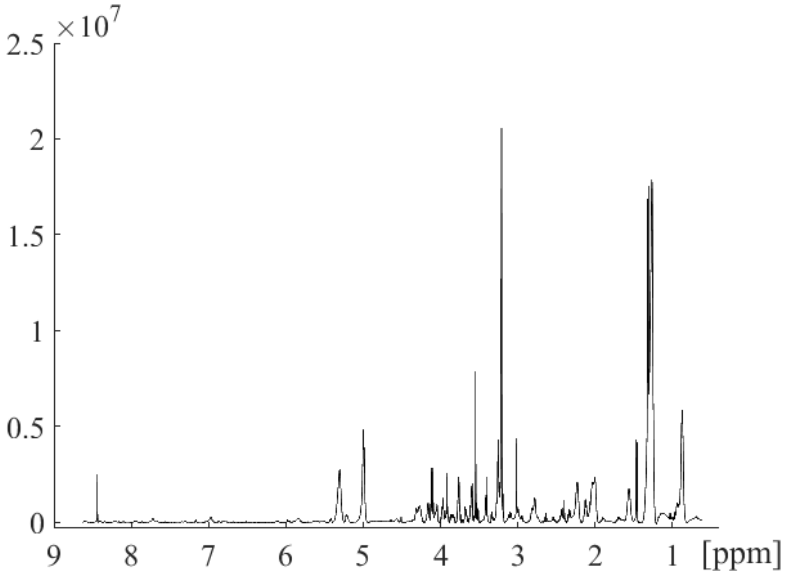

Figure C.15: ^{1}H HR-MAS MR spectrum of basal-like PDX tissue from CB-839 treated mouse no. 4.

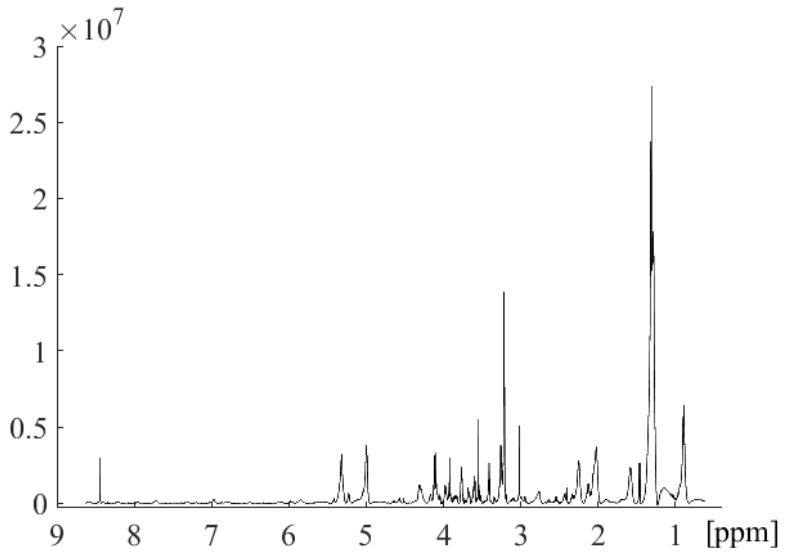

Figure C.16: ^{1}H HR-MAS MR spectrum of basal-like PDX tissue from CB-839 treated mouse no. 5.

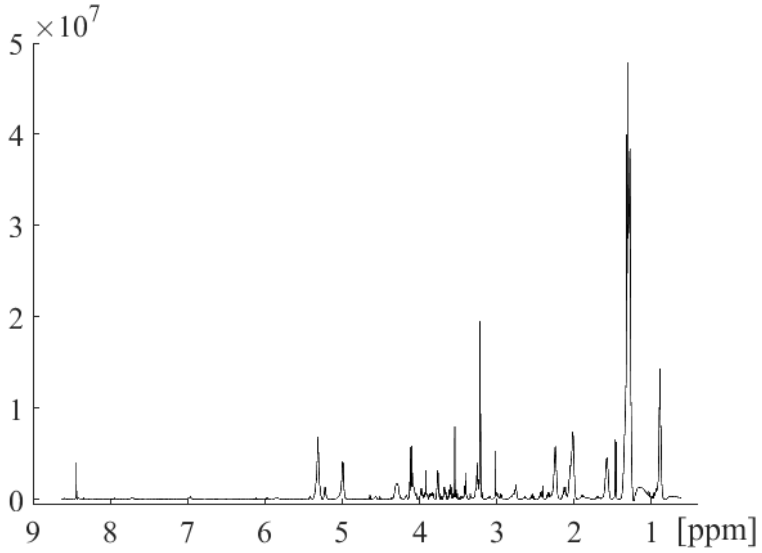

Figure C.17: ^{1}H HR-MAS MR spectrum of basal-like PDX tissue from CB-839 treated mouse no. 6.

C.4 ^{1}H MR spectra of controls from basal-like PDX tissue

^{1}H MR spectra of basal-like PDX tissue from control mice.

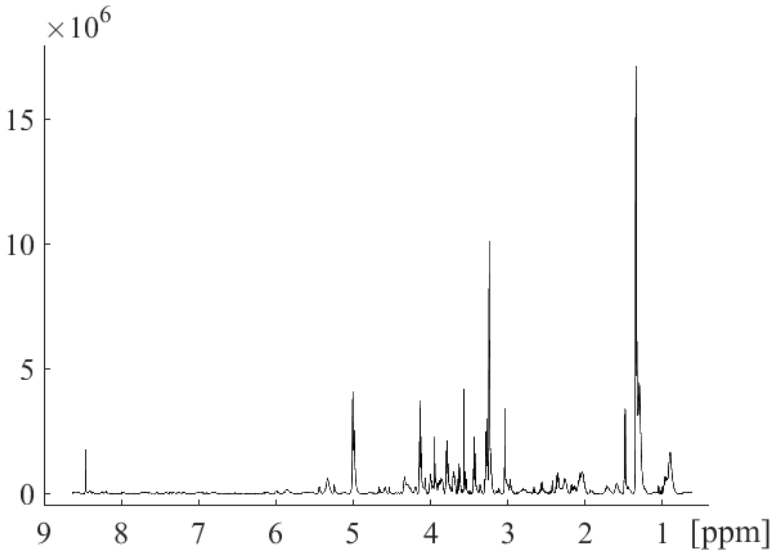

Figure C.18: ^{1}H HR-MAS MR spectrum of basal-like PDX tissue from control mouse no. 7.

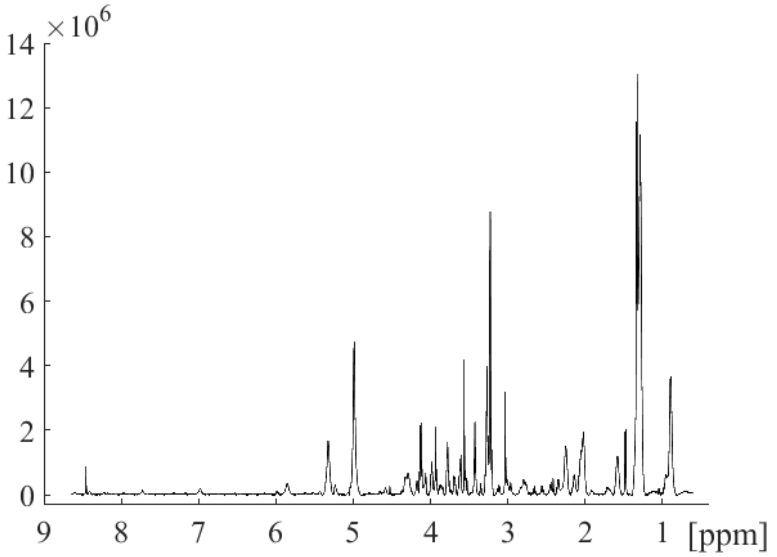

Figure C.19: ^{1}H HR-MAS MR spectrum of basal-like PDX tissue from control mouse no. 8.

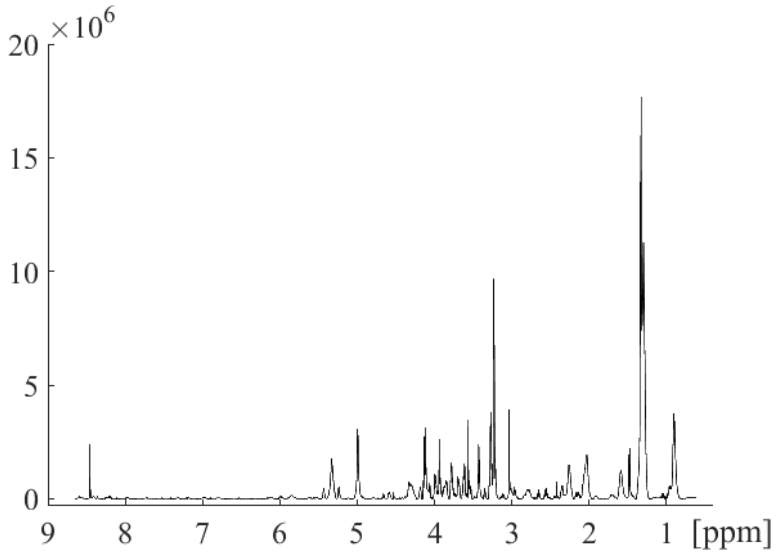

Figure C.20: ^{1}H HR-MAS MR spectrum of basal-like PDX tissue from control mouse no. 9.

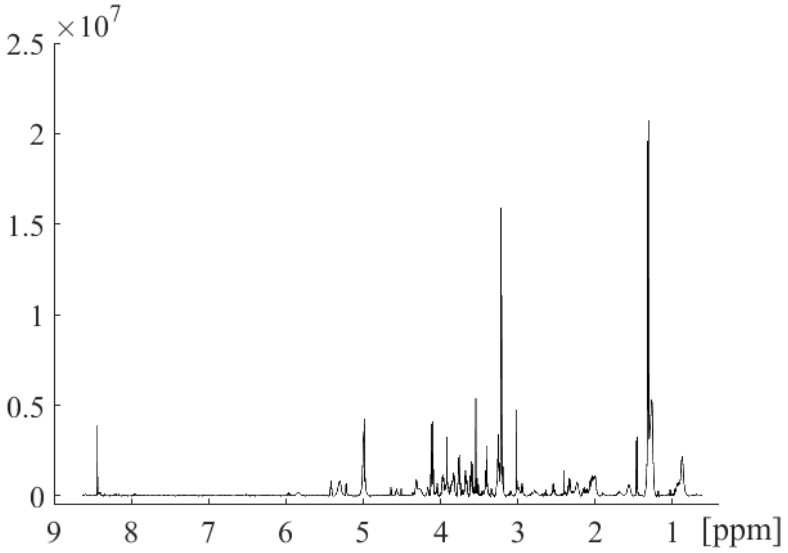

Figure C.21: ^{1}H HR-MAS MR spectrum of basal-like PDX tissue from control mouse no. 10.

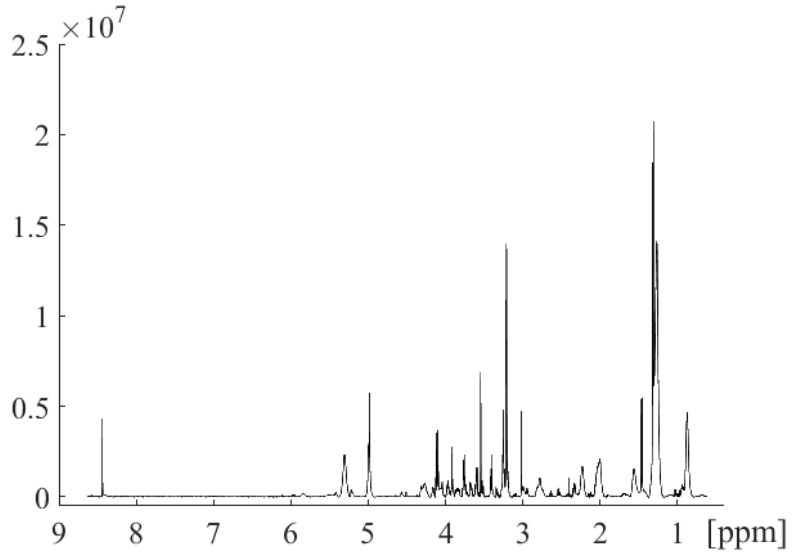

Figure C.22: ^{1}H HR-MAS MR spectrum of basal-like PDX tissue from control mouse no. 11.

C.5 ^{13}C MR spectra of serum from basal-like PDX mice treated with CB-839

^{13}C MR spectra of serum from mice treated with CB-839 with basal-like PDXs.

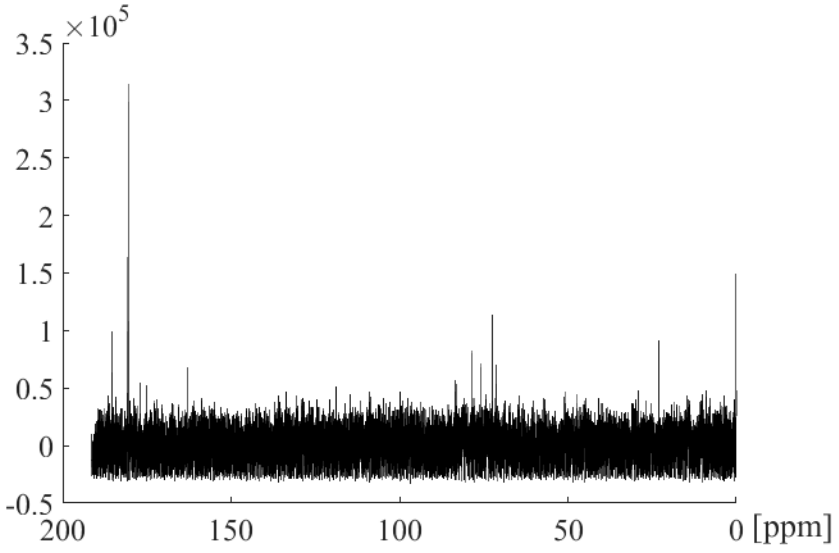

Figure C.23: ^{13}C MR spectrum of serum from mouse no. 1 with basal-like PDX, treated with CB-839.

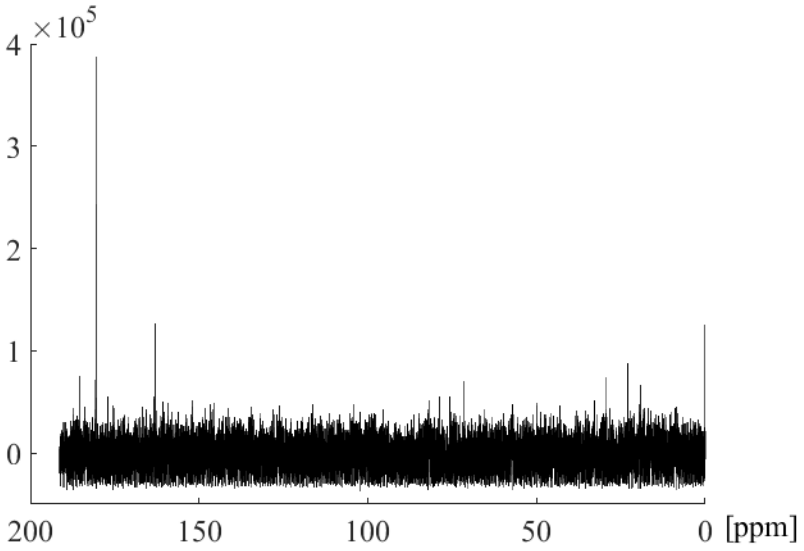

Figure C.24: ^{13}C MR spectrum of serum from mouse no. 2 with basal-like PDXs, treated with CB-839.

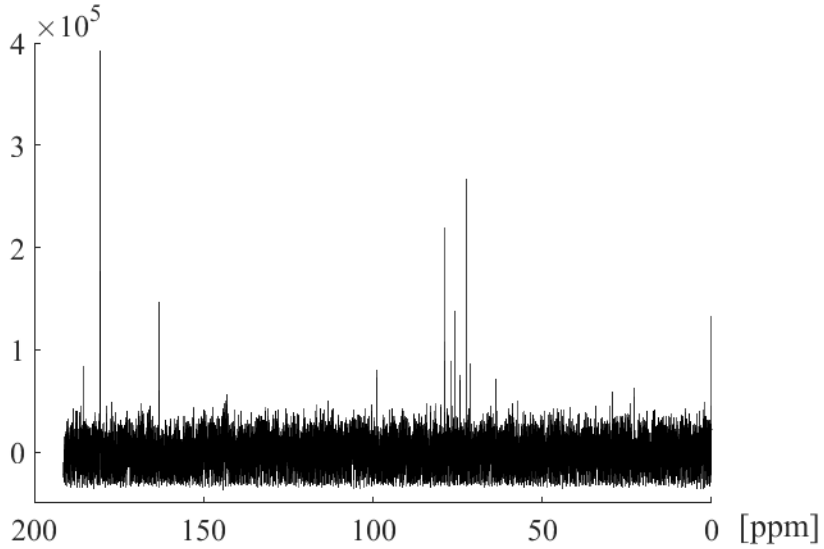

Figure C.25: ^{13}C MR spectrum of serum from mouse no. 3 with basal-like PDXs, treated with CB-839.

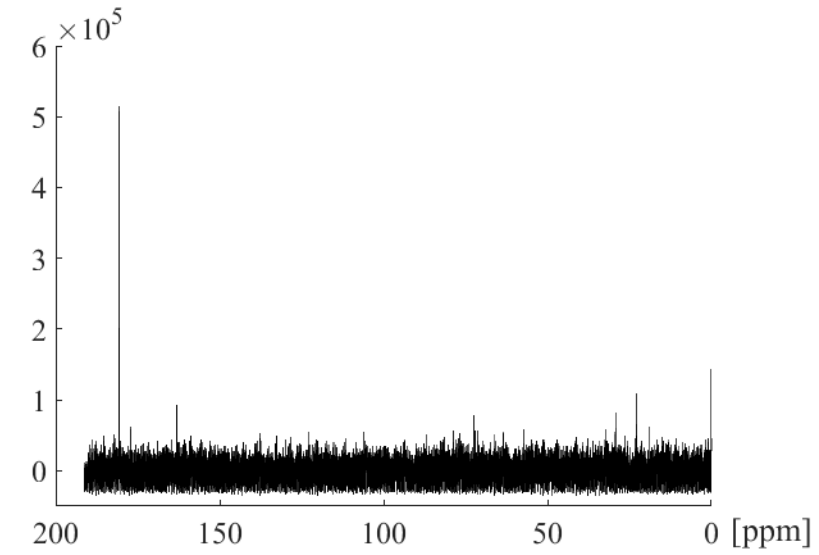

Figure C.26: ^{13}C MR spectrum of serum from mouse no. 4 with basal-like PDXs, treated with CB-839.

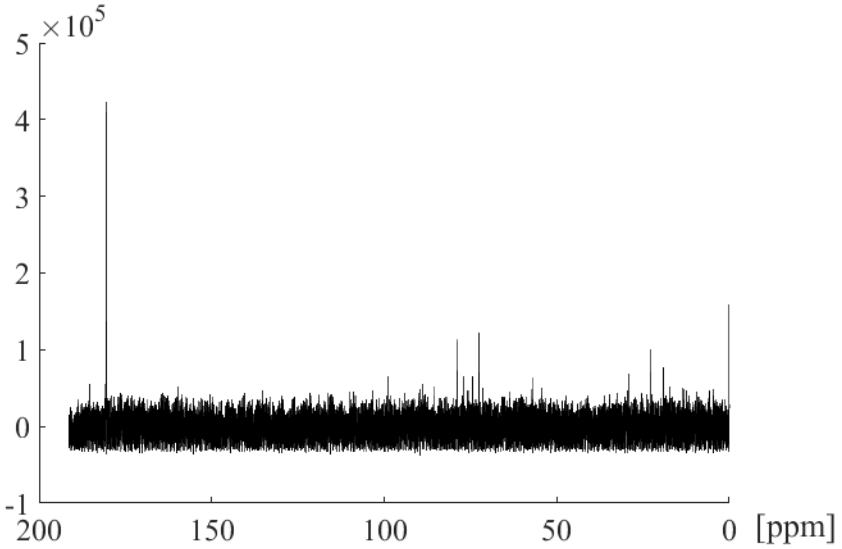

Figure C.27: ^{13}C MR spectrum of serum from mouse no. 5 with basal-like PDXs, treated with CB-839.

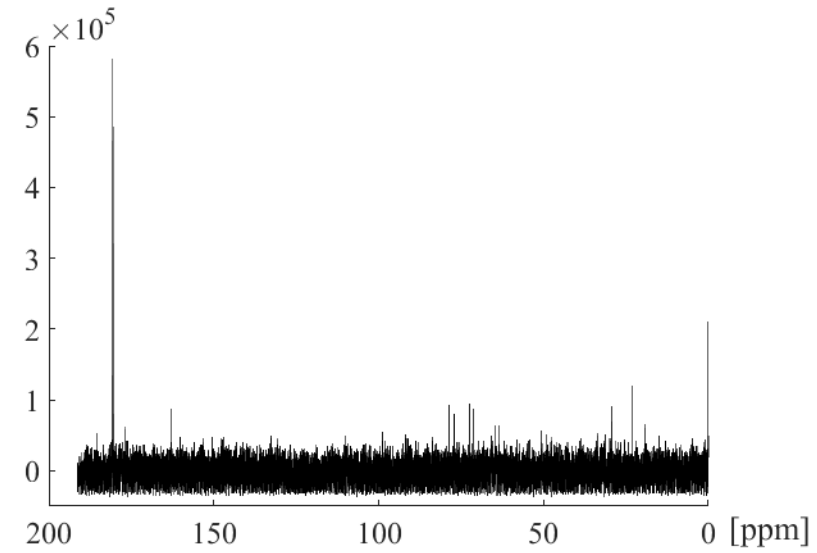

Figure C.28: ^{13}C MR spectrum of serum from mouse no. 6 six with basal-like PDXs, treated with CB-839.

C.6 ^{13}C MR spectra of serum from control mice with basal-like PDXs

^{13}C MR spectra of serum from control mice with basal-like PDXs.

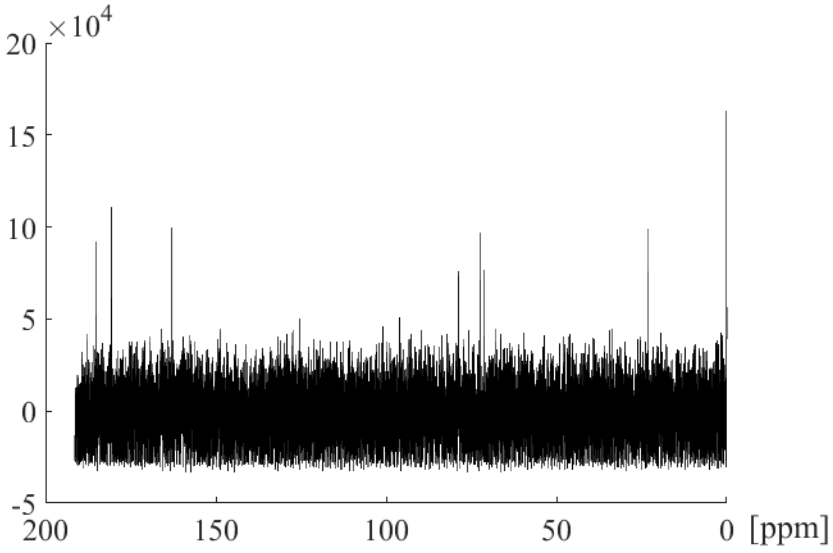

Figure C.29: ^{13}C MR spectrum of serum from control mouse no. 7 with basal-like PDXs.

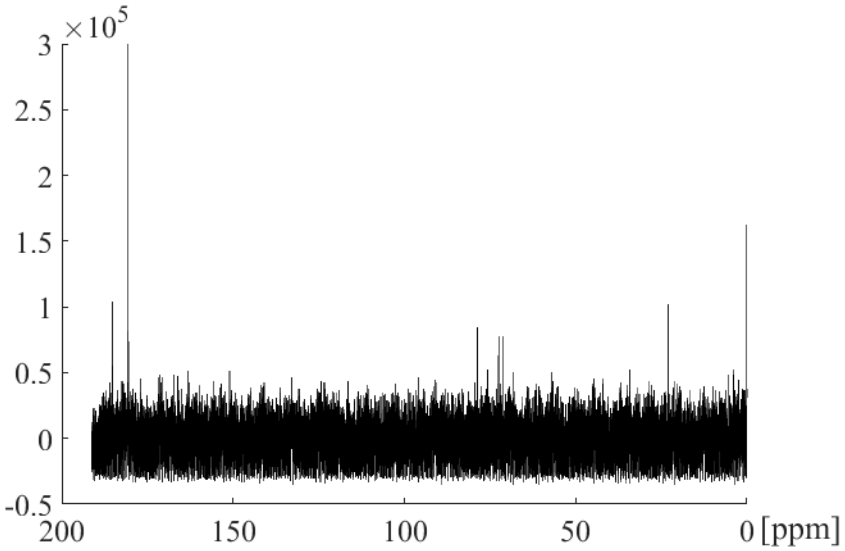

Figure C.30: ^{13}C MR spectrum of serum from control mouse no. 8 with basal-like PDXs.

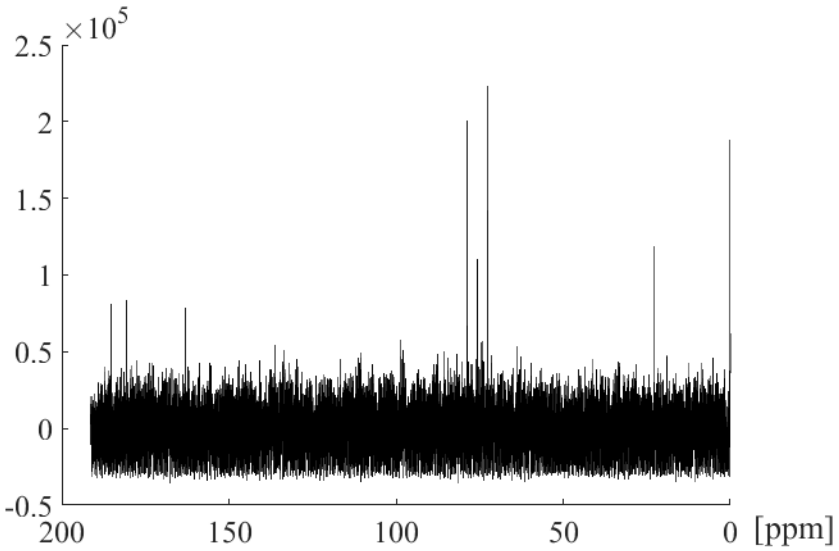

Figure C.31: ^{13}C MR spectrum of serum from control mouse no. 9 with basal-like PDXs.

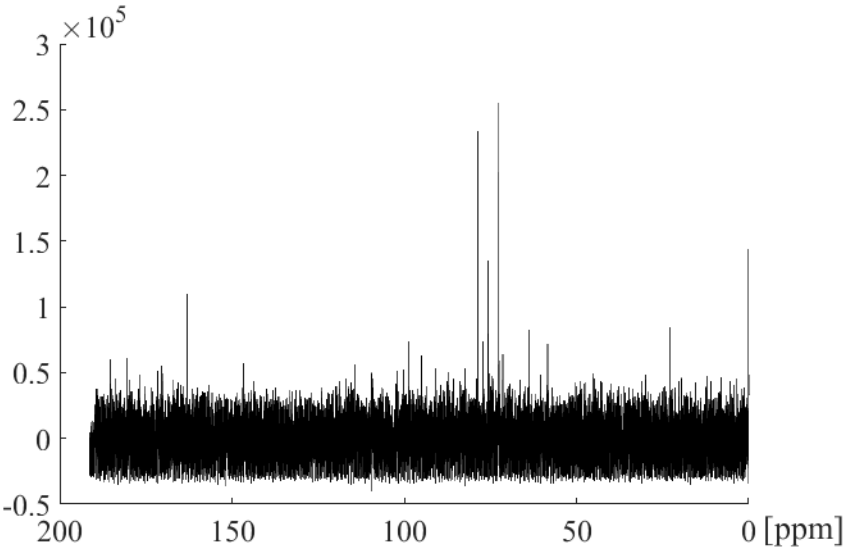

Figure C.32: ^{13}C MR spectrum of serum from control mouse no. 10 with basal-like PDXs.

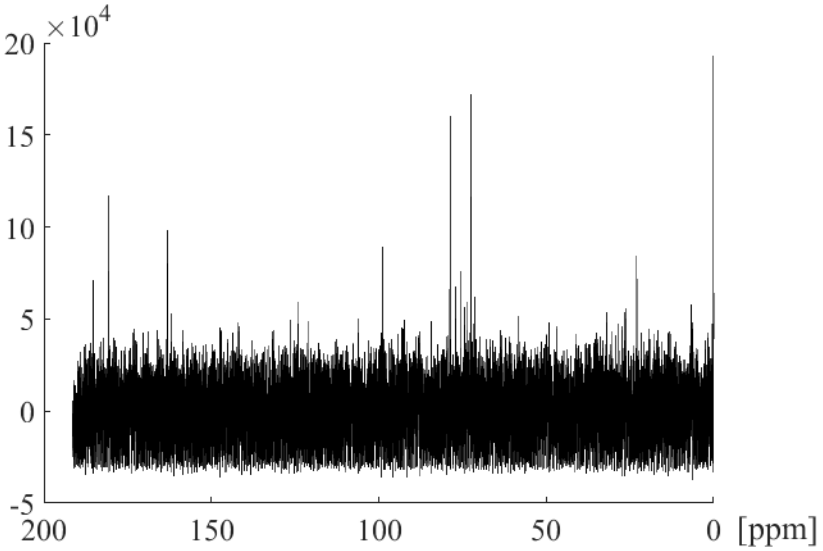

Figure C.33: ^{13}C MR spectrum of serum from control mouse no. 11 with basal-like PDXs.

D Normal Q-Q plots

Normal Q-Q plots were plotted using SPSS (IBM) of integral values of selected metabolites in ^{13}C MR spectra of basal-like PDX tissue.

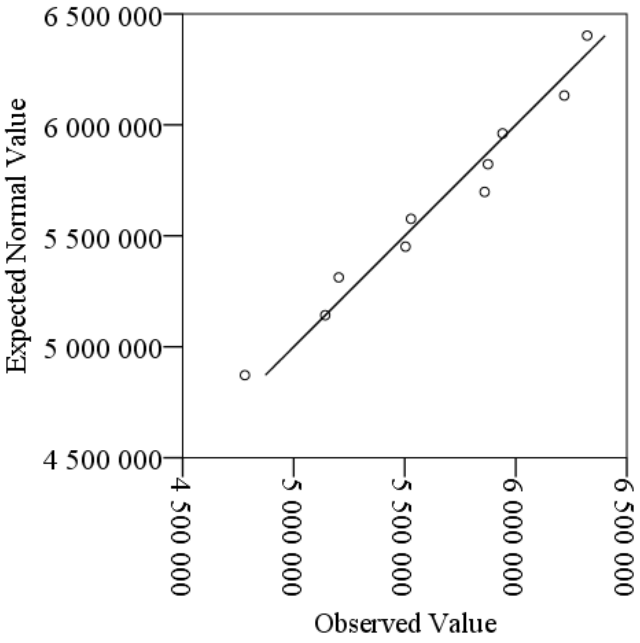

Figure D.1: Normal Q-Q plot of integral values of L-lactate(C5) from ^{13}C MR spectra of basal-like PDX tissue.

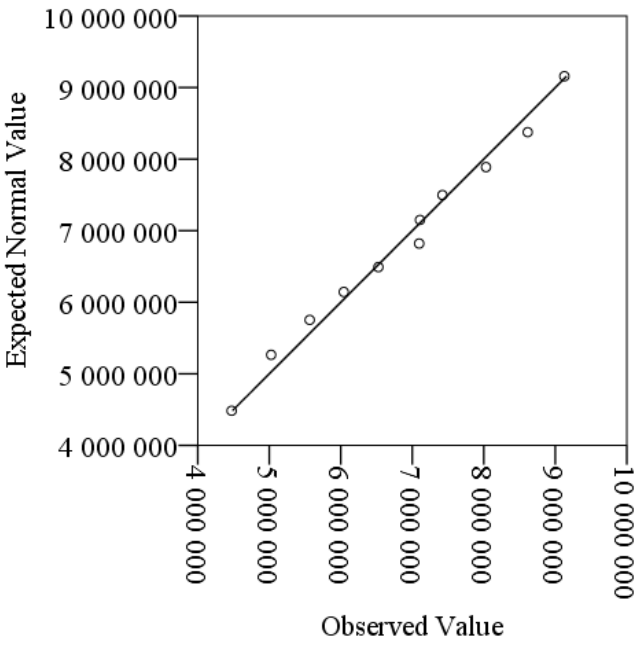

Figure D.2: Normal Q-Q plot of integral values of L-glutamate(C5) from ^{13}C MR spectra of basal-like PDX tissue.

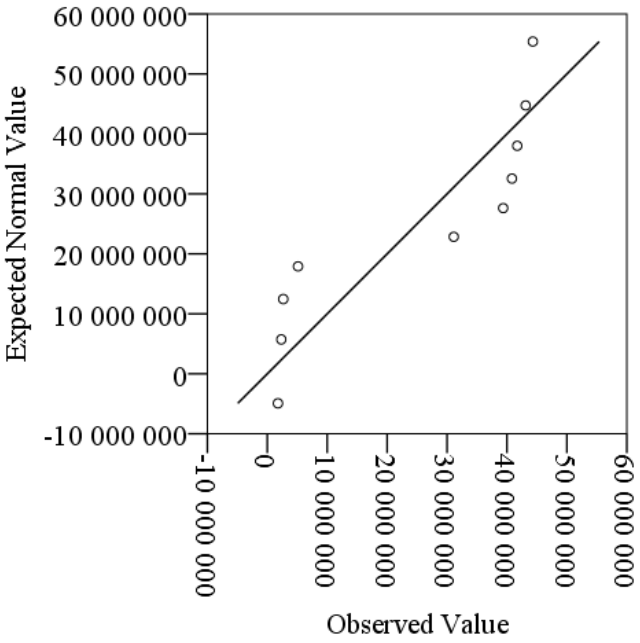

Figure D.3: Normal Q-Q plot of integral values of L-glutamine(C5) from ^{13}C MR spectra of basal-like PDX tissue.

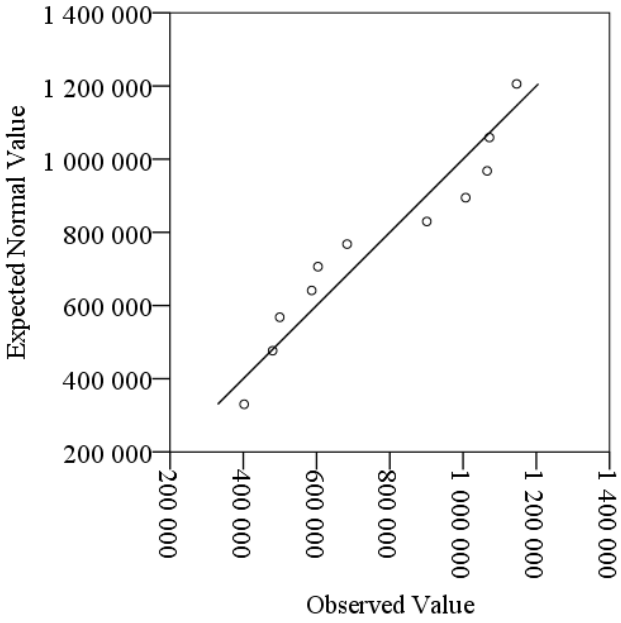

Figure D.4: Normal Q-Q plot of integral values of L-lactate(C1) from ^{13}C MR spectra of serum from mice with basal-like PDXs.

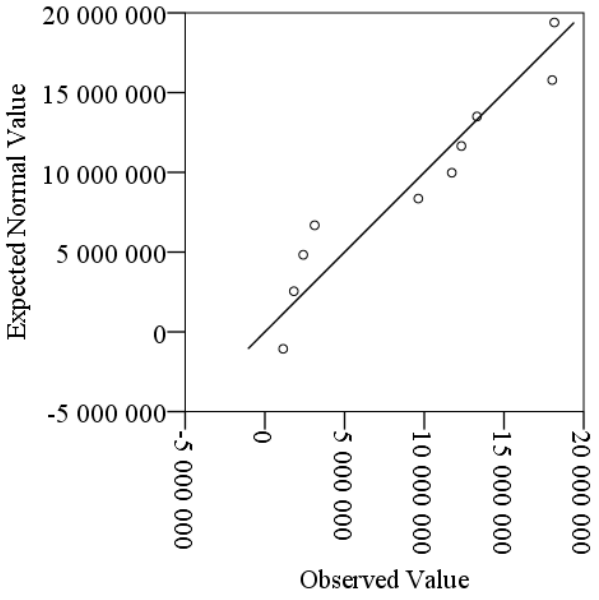

Figure D.5: Normal Q-Q plot of integral values of L-glutamine(C5) from ^{13}C MR spectra of serum from mice with basal-like PDXs.

E Tumor growth of in MAS98.12 tumors when treated with CB-839

Results from a previous, unpublished study on tumor growth of basal-like PDX model MAS98.12 in immunodeficient mice, where tumors were orthotopically implanted in the mammary fat pad (FOTS ID: 7713). Results of tumor growth, after treatment with CB-839 or controls, are shown in Figure E.1.

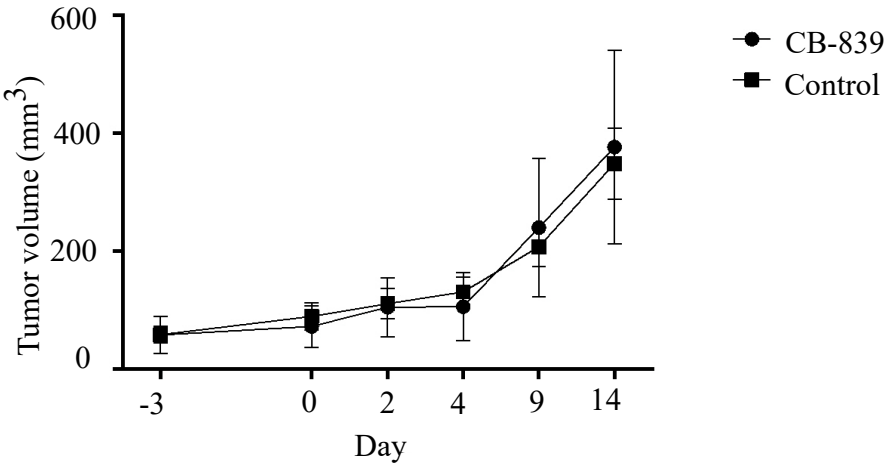

Figure E.1: Tumor volume of basal-like PDX tumors ($n = 6$) implanted in immunodeficient mice at different days after different times of treatment with CB-839 or controls.

Figure E.1 show no impact on tumor volume of basal-like MAS98.12 tumors when treated with CB-839 compared with the controls.